Decoding potential effects of climate and vegetation change on mineral weathering in alpine soils: An experimental study in the Wind River Range (Wyoming, USA)

Mavris, Christian ; Furrer, Gerhard ; Dahms, Dennis ; Anderson, Suzanne P ; Blum, Alex ; Goetze, Jens ; Wells, Aaron ; Egli, Markus

Abstract: Climate change and a related increase in temperature, particularly in alpine areas, force both flora and fauna to adapt to the new conditions. These changes should in turn affect soil formation processes. The aim of this study was to identify possible consequences for soils in a dry-alpine region with respect to weathering of primary minerals and leaching of elements under expected vegetation and climate changes. To achieve this, a field empirical approach investigating an altitudinal sequence was used in combination with laboratory weathering experiments simulating several scenarios. The study sites are located in Sinks Canyon and Stough Basin of the Wind River Range, Wyoming, USA. The following sites (from moist to dry with increasing temperature along the sequence) were investigated: 10 soil profiles (Typic Haplocryoll) in a tundra ecotone, 10 soil profiles (Ustic Haplocryoll) in a pine-fir forest and 20 soil profiles (Ustic Argicryoll) in sagebrush. All soils developed on granitoid moraines. Soil mineralogy was analysed using cathodoluminescence and X-ray diffraction. This revealed that biotite and plagioclase were both weathered to smectite while plagioclase also weathered to kaolinite. Cooler, wetter, altitude-dependent conditions promoted weathering of primary minerals. Furthermore, the soils of the tundra and forest zone exhibited a higher acidity and more organic carbon. In a series of wet laboratory batch experiments, materials from topsoils (A horizons) and subsoils (B horizons) in each ecotone were examined alone or in combination with other samples. In a first step, aqueous extracts of the topsoil samples were generated in batch reactors and analysed for the main ions. In a second and a third step the topsoil extracts were reacted with the subsoil samples of the same ecotone, and with the subsoil samples of the ecotones at higher altitude. The total duration of these batch experiments was 1800 h, and the solutes were measured using ICP-OES and ion chromatography. Dissolved Ca, Mg and K were mainly controlled by the chemical weathering of oligoclase, K-feldspar and biotite. With increasing altitude the total concentrations of Ca, Mg and K in the aqueous extracts decreased, the relative ionic contribution from K decreased, while the ionic contribution from Ca increased. Climate change (warming, changed precipitation) potentially will reduce weathering intensity, soil acidity and the content of organic carbon. An altitudinal shift in vegetation due to climate change seems to affect the ionic composition of the soil solution. In the case of a shift from forest to sagebrush and tundra to forest or sagebrush, the relative contribution from K would increase at the expense of Ca. We hypothesise that K will play an important role in future biogeochemical cycles under the assumptions of climate warming and subsequent vegetation shifts to higher altitudes.

DOI: https://doi.org/10.1016/j.geoderma.2015.04.014

Originally published at:
Mavris, Christian; Furrer, Gerhard; Dahms, Dennis; Anderson, Suzanne P; Blum, Alex; Goetze, Jens; Wells, Aaron; Egli, Markus (2015). Decoding potential effects of climate and vegetation change on mineral weathering in alpine soils: An experimental study in the Wind River Range (Wyoming, USA). Geoderma, 255-256:12-26.
DOI: https://doi.org/10.1016/j.geoderma.2015.04.014

Decoding potential effects of climate and vegetation change on mineral weathering in alpine soils: An experimental study in the Wind River Range (Wyoming, USA)

Christian Mavris[1,2,4], Gerhard Furrer[2], Dennis Dahms[3], Suzanne P. Anderson[4], Alex Blum[5], Jens Goetze[6], Aaron Wells[7], Markus Egli[8]*

[1]Department of Earth Sciences, Natural History Museum, Cromwell Road, London SW7 5BD, U.K.
[2]Institute of Biogeochemistry and Pollutant Dynamics (IBP), ETH Zurich, CH-8092, Switzerland
[3]Department of Geography, University of Northern Iowa, Cedar Falls, USA
[4]INSTAAR and Dept. of Geography UCB-450, University of Colorado, Boulder, CO 80309, USA
[5]US Geological Survey, 3215 Marine Street, Boulder, CO 80303, USA
[6]Department of Mineralogy, TU Bergakademie Freiberg, D-09596 Freiberg, Germany
[7] ABR, Inc. Environmental Research and Services, P.O. Box 240268, Anchorage, AK, 99524
[8]Department of Geography, University of Zurich, CH-8057, Switzerland

*Corresponding author. Tel.: +41 44 635 51 14; fax: +41 44 6356848.
E-mail address: markus.egli@geo.uzh.ch (M. Egli).

Abstract

Climate change and a related increase in temperature, particularly in alpine areas, force both flora and fauna to adapt to the new conditions. These changes should in turn affect soil formation processes. The aim of this study was to identify possible consequences for soils in a dry-alpine region with respect to weathering of primary minerals and leaching of elements under expected vegetation and climate changes. To achieve this, a field empirical approach investigating an altitudinal sequence was used in combination with laboratory weathering experiments simulating

several scenarios. The study sites are located in Sinks Canyon and Stough Basin of the Wind River Range, Wyoming, USA. The following sites (from moist to dry with increasing temperature along the sequence) were investigated: 10 soil profiles (Typic Haplocryoll) in a tundra ecotone, 10 soil profiles (Ustic Haplocryoll) in a pine-fir forest and 20 soil profiles (Ustic Argicryoll) in sagebrush. All soils developed on granitoid moraines. Soil mineralogy was analysed using cathodoluminescence and X-ray diffraction. This revealed that biotite and plagioclase were both weathered to smectite while plagioclase also weathered to kaolinite. Cooler, wetter, altitude-dependent conditions promoted weathering of primary minerals. Furthermore, the soils of the tundra and forest zone exhibited a higher acidity and more organic carbon.

In a series of wet laboratory batch experiments, materials from topsoils (A horizons) and subsoils (B horizons) in each ecotone were examined alone or in combination with other samples. In a first step, aqueous extracts of the topsoil samples were generated in batch reactors and analysed for the main ions. In a second and a third step the topsoil extracts were reacted with the subsoil samples of the same ecotone, and with the subsoil samples of the ecotones at higher altitude. The total duration of these batch experiments was 1800 hours, and the solutes were measured using ICP-OES and ion chromatography. Dissolved Ca, Mg and K were mainly controlled by the chemical weathering of oligoclase, K-feldspar and biotite. With increasing altitude the total concentrations of Ca, Mg and K in the aqueous extracts decreased, the relative ionic contribution from K decreased, while the ionic contribution from Ca increased.

Climate change (warming, changed precipitation) potentially will reduce weathering intensity, soil acidity and the content of organic carbon. An altitudinal shift in vegetation due to climate change seems to affect the ionic composition of the soil solution. In the case of a shift from forest to sagebrush and tundra to forest or sagebrush, the relative contribution from K would increase at the expense of Ca. We hypothesise that K will play an important role in future biogeochemical cycles under the assumptions of climate warming and subsequent vegetation shifts to higher altitudes.

Keywords

Climate change, weathering, feldspar, vegetation change, Wind River Range, alpine region

56

57 ## Introduction

58 Mountain ecosystems are, for several reasons, likely to be especially responsive to changing
59 environmental conditions such as global warming, acid deposition and atmospheric nutrient inputs
60 (Theurillat et al., 1998; Arn, 2002; Hosein et al., 2004; Seastedt et al., 2004). Ecosystems in turn
61 affect soil-forming processes (Amundson et al., 2007), particularly through their impact on
62 chemical weathering rates. The rates of chemical weathering reactions and their dependencies on
63 environmental factors are of fundamental interest for understanding soil systems and their inter-
64 relations with surrounding environments.

65 Dissolution of most primary rock-forming minerals is limited by slow kinetics at the mineral–water
66 interfaces (Stumm and Morgan, 1996). Mineral dissolution rates depend on *extrinsic* factors such
67 as T, pH, Eh, and exudates from microbes and plant roots, as well as on *intrinsic* factors such as
68 mineral-surface properties and the presence of weathering products. Acidity and the availability of
69 ligands promote dissolution reactions for primary minerals and govern their transformations into
70 secondary minerals (Furrer et al., 1990; Wehrli et al., 1990; Sverdrup and Warfvinge, 1993; Mavris
71 et al., 2010). Erosion provides materials with an easily weatherable surface and consequently is a
72 primary intrinsic influence in the soil system. Chemical weathering and physical erosion are
73 coupled to the degree that mineral weathering rates depend on the availability of fresh mineral
74 surfaces with high reactivity (White et al., 1999; Jacobson and Blum, 2003; Riebe et al., 2004;
75 Dixon and von Blanckenburg, 2012; Heimsath et al., 2012; Heimsath, 2014; Larsen et al., 2014).

76 One obvious expression of environmental change due to climatic warming is the altitudinal shift of
77 vegetation and related ecological associations (Di Pasquale et al., 2008; Berthel et al., 2012; Solàr,
78 2013). Muhs et al. (2001) concluded that weathering rates are influenced primarily by a
79 combination of precipitation, temperature and parent rock material; however, higher temperatures
80 do not necessarily lead to increased weathering rates in alpine regions (Egli et al., 2003). The
81 empirical effects of the climate factor on weathering rates, mineral formation, and transformation
82 remain equivocal and are still a matter of debate (e.g., Óskarsson et al., 2012; Lybrand and
83 Rasmussen, 2014). While some demonstrate that temperature is the dominant variable exerting

control on the extent of weathering (e.g. Óskarsson et al., 2012), others emphasise or hypothesise the particular role of water availability in the soils and biological processes (e.g. White and Blum 1995; White et al. 1999; Dixon et al. 2009;Williams et al. 2010; Brantley et al., 2011; Rasmussen et al. 2011; etc.). Patterns of weathering processes in alpine environments are strongly linked to biological and microclimatic factors (Egli et al., 2010). Climate warming can give rise to short-term changes in the distribution of vegetation and may induce soil chemical and mineralogical changes within a relatively short period of time (Zanelli et al., 2006; 2007).

Investigations in dry alpine regions concerning the effects of climate change on mineral weathering are mostly lacking. Sagebrush steppe and lodgepole pine forests are two of the most widespread vegetation types on mountain areas of the western United States (Bradford et al., 2014; Wells et al., in press). Climate warming may reduce snowpack, increase evaporation and transpiration, and lengthen the duration of dry soil conditions during summer (Adams et al., 2009). Changes in climate and soil-conditions will affect the distribution of sagebrush and lodgepole pine vegetation (Bradford et al., 2014) that, in turn, will likely alter weathering conditions in the soils.

Consequently, the aim of this investigation was to decipher potential changes in weathering mechanisms caused by a vegetation shift (as a consequence of expected climate warming). We chose Stough Basin and Sinks Canyon (Wind River Range, central Rocky Mountains, USA) for this research because this area is surrounded in the east, west, and south by the high semi-desert Green River, Wind River, and Great Divide basins. As a consequence, regional climate warming in this region should have a relatively direct effect on ecotone migration along this alpine-montane-tundra ecological transect. Two treelines exist here: a lower treeline, below which sagebrush-steppe is dominant and tree growth is moisture- limited and a higher treeline, which is temperature-limited. It is expected that in the future, the elevations of both of these treelines will gradually shift upwards (Wells et al., in press).

Study area

Sinks Canyon and the Stough Creek Basin, in the SE Wind River Range (WRR), Wyoming, were

112 selected for this investigation because the important ecotones are very well expressed here. In this
113 area, the positions of lower and upper treeline are approximately 2200 – 2600 (lower limit;
114 depending on exposition and amount of annual precipitation) and 3200 – 3300 m, respectively
115 (Wells et al., in press). Following the Wells et al. delineations, we divided the area into three main
116 ecological zones: a subarid environment that is mainly populated by sagebrush (≤ 2400 m asl), a
117 pine-fir montane forest zone (2400 – 3200 m asl), and a tundra zone (> 3200 m asl).
118 The bedrock lithology in the south-eastern core of the WRR is dominated by Archean-Precambrian
119 granites and granodiorites associated with the Louis Lake batholith (Love and Christiansen, 1985;
120 Frost et al., 2000; Dahms, 2004; Dahms et al., 2012). Paleozoic limestones/dolomites and
121 sandstones cover the Precambrian units on the lower mountain slopes below ~2600 m (Love et al.,
122 1992; Dahms, 2004). It was into these units that Sinks Canyon formed in response to Laramide
123 deformation in this region (Wise, 1963; Erslev, 1986).
124 Sinks Canyon is located southwest of Lander, on the SE flank of the range (Fig. 1). The canyon is
125 the most southerly of the four canyons along the eastern slope of the WRR where Pleistocene
126 glacial deposits have been described (e.g. Chadwick et al., 1997; Phillips et al., 1997; Dahms et
127 al., 2002; Dahms, 2004; Fabel et al., 2004; Züst et al., 2014). In this study, we sampled soil profiles
128 from a combination of Pinedale and Bull Lake-age moraines on the canyon's north wall at
129 elevations between 2000 – 2500 m asl (Dahms, 2004).
130 Stough Creek Basin lies at the head of the basin of the Middle Fork of the Popo Agie River,
131 approximately 17 km upstream of Sinks Canyon. It lies directly below the Continental Divide
132 roughly between Atlantic and Wind River peaks. Soils sampled from the basin are developed in
133 post-LGM granitic glacial tills. Depending on the vegetation zone, the soils are classified within the
134 U.S Soil Taxonomy (Soil Survey Staff, 2014) as Ustic Argicryolls (sagebrush), Ustic Haplocryolls
135 (forest zone) and Typic Haplocryolls (tundra).
136
137
138 **Material and methods**
139

Soil sampling strategy

Soil sampling was carried out relative to the dominant ecological zones (Wells et al., in press; Table 1). Soils were described and sampled from hand-dug pits using standard methods and horizon nomenclature (Schoeneberger et al., 2012). Pits were excavated to a depth of ~40 cm but we typically sampled only the A and B horizons. We sampled occasional C horizons in order to obtain reference materials for parent material characteristics. In order to understand soil variability, 20 sites in the sagebrush-ecotone zone, 10 sites in the forest and 10 sites in the tundra zone (Fig. 2) were sampled (Fig. 1). Approximately 1 kg of material was collected from each horizon.

Soil physical and chemical characters

The weight proportion of soil skeleton was determined by sieving the bulk soil material (2 mm sieve). The grain size distribution was measured on all samples after oxidation of organic matter with H_2O_2 30% (Dahms (2002) after Singer and Janitzky, 1986). The clay fraction (< 2 µm) was then separated gravimetrically from the silt-clay slurry (< 63 µm). The silt fraction (2 – 63 µm) was then weighted and stored for X-ray diffraction analyses.

Soil pH (in 0.01 M $CaCl_2$) was determined on air-dried fine earth samples using a soil/solution ratio of 1/2.5. Organic matter (OM) and carbonate ($CaCO_3$) content were determined gravimetrically after sequential dry combustion in a muffle furnace at 550 °C and 950 °C (Dean, 1974; Heiri et al., 2001).

Mineralogy

The mineralogical composition of the soil samples from all sites was determined using X-ray diffraction analysis on randomly oriented specimens of the fine earth and silt fraction. X-ray measurements were carried out using a Siemens D500 XRD, with CuKα radiation (40 kV, 30 mA), a graphite monochromator and a step width of 0.02°2θ. The patterns were measured in the range of 4 – 70° 2θ, with a counting time of 1 s. For XRD analysis, the bulk material was milled for 5 minutes in ethanol with a McCrone micronising mill. After milling, the sample (< 20 µm) was dried at 60 °C.

168 Quantitative mineral distribution was determined by adding corundum as an internal standard (15
169 wt%, Mavris et al., 2010) in order to avoid the overwhelming diffraction peaks of biotite and
170 hornblende. The quantification was performed using the macro code 'Rockjock' (Eberl, 2004;
171 Christidis et al., 2006). The program compares integrated XRD intensities for minerals present in
172 the sample, and weight percents are calculated from previously measured mineral intensity ratios
173 (Eberl, 2004).
174
175 *Cathodoluminescence (CL)*
176 The fine earth fraction of the parent material was washed, organic matter (density < 1 g/cm^3)
177 removed by flotation in deionised water and then air-dried. The grains were embedded in polyester
178 resin and sliced to a thickness of ca. 30 µm. Sample preparation was conducted at OMT
179 Petrographic Lab, Aosta, Italy.
180 CL measurements were done on carbon-coated, polished thin sections using a 'hot cathode' CL
181 microscope HC1-LM (Neuser et al., 1995). The system was operated at 14 kV accelerating voltage
182 and a current of 0.2 mA (current density of about 10 µA/mm^2). Luminescence images were
183 captured 'on-line' during CL operations using a peltier cooled digital video-camera (OLYMPUS
184 DP72). CL spectra in the wavelength range 380 to 1000 nm were recorded with an Acton
185 Research SP-2356 digital triple-grating spectrograph with a Princeton Spec-10 CCD detector that
186 was attached to the CL microscope by a silica-glass fiber guide. CL spectra were measured under
187 standardized conditions (wavelength calibration by a Hg-halogen lamp, spot width 30 µm,
188 measuring time 2 s).
189
190 *Dissolution experiments*
191 In order to compare the dissolution behaviour of the soils of the different ecotones and to simulate
192 a vegetation change due to climate warming, a series of batch experiments were performed with
193 top- and subsoil fine earth samples. In a first step, a water extract (deionised H_2O) of the topsoils
194 was prepared and collected. An aliquot of this extract was then added to the topsoil samples and
195 the release of ions was measured during the experiment. Furthermore, a second aliquot of the

196 topsoil water extract was added to the fine earth of its own subsoil (B-horizon). In addition, to
197 simulate a vegetation change (caused by climate warming), the effect of the topsoil liquid extracts
198 (using a third aliquot) on the higher altitude subsoil samples was investigated. The extract of the A
199 horizon of the sagebrush site S(A) was applied to the B horizons of the forest F(B) and tundra site
200 T(B). Similarly, the topsoil extract of the forest site F(A) was applied to the tundra subsoil T(B). The
201 corresponding scheme is given in Fig. 3.
202 In detail, the procedure was the following: To perform the experiments, 2.0 litre extract of S(A), 1.5
203 litre of F(A) and 1.0 litre of T(A) had to be prepared. The water extract was obtained by stirring at
204 room temperature the topsoil with deionized H_2O using a soil:water ratio of 1:5. The solutions were
205 then filtered (0.45 µm cellulose nitrate filters) and centrifuged (2000 rpm for 40 min). Subsequently,
206 the topsoil extracts were added to the top- and subsoil samples at a water:soil ratio of 5:1, run for
207 1800 hours and sampled at intervals. To prevent microbial degradation of the organic compounds,
208 AgCl was added to all solutions.
209 All batch reactors consisted of 1L acid washed (1M HCl) amber glass bottles. The vessels were
210 gently shaken on an orbital shaking table (approx. 120 rpm). Active temperature control was used,
211 as the reactors were placed in a Lunaire environmental chamber with constant temperature (50 °C)
212 for the entire duration of the experiment. The bottles were closed with a double layer of Parafilm©
213 membrane to prevent evaporation of the solution over the experimental time.
214 All solutions were analysed using ICP-OES to determine major cationic concentrations (Ca, Mg, K,
215 Na, Fe, Sr, Al and Si). Ion chromatography (IC) was employed to measure the content of major
216 anions (NO_3^-, SO_4^{2-} and Cl^-).
217
218 *Statistics*
219 The individual datasets were checked for normal distribution using a Shapiro-Wilk test (SigmaPlot
220 11.0 (Systat Software Inc.); Jann, 2005). This procedure was checked using a two-tailed test for
221 significance. Depending on the data distribution the Pearson or Spearman rank correlation
222 coefficient was calculated. Analysis of variance (ANOVA) or a Kruskal-Wallis test (non-normal
223 distribution) was performed in order to test differences among groups. For all tests a level of

224 significance of 0.05 was considered.

225

226

227 **Results**

228 *Soils characteristics*

229 All soils had textures of loamy sand or sandy loam (Tables 2 and 3). At the sagebrush sites, the
230 majority of the plant roots were concentrated at the top 10 – 15 cm; at all other sites roots were
231 concentrated in the topsoil but also found even below 40 cm. In the A-horizons (Fig. 4), the highest
232 mean pH value (5.07) was measured at the sagebrush (S) sites, followed by the tundra (T) with
233 4.82 and then by the more acidic forest (F) sites (3.96). The average pH value of the parent
234 material samples (labelled as 'C' in Fig. 4) was 4.84. The differences among the sites were
235 statistically significant ($p < 0.05$).

236 No weight difference was observed between LOI values generated at 550 °C and those generated
237 at 950 °C (thus, no carbonate was present in the soils). LOI represents in this case only soil
238 organic matter and interstitial H_2O in any hydrated minerals (Fig. 4). With increasing soil depth, LOI
239 values decreased from 3 – 4 % in the A-horizons to < 2% in B-horizons and 0.76 % in C-horizons
240 (parent material). A-horizons at sagebrush sites had the lowest organic matter content (3.13 %),
241 followed by the tundra (3.91 %) and the forested sites (4.32 %). The differences in organic matter
242 content in the A horizon between the different ecotones are statistically significant only between
243 the sagebrush and the tundra ecotones. Values for tundra and forest A-horizons do not statistically
244 differ. In the subsoil, all ecotones significantly differed from each other with the tundra having the
245 highest soil organic matter content.

246

247 *Soil mineralogy*

248 The mineralogy of the investigated soils reflects the granitoid character of the moraine deposits. X-
249 ray diffraction (evaluated using the RockJock macro model) indicated the presence of quartz, K-
250 feldspar (microcline), Na-rich plagioclase (oligoclase), amphibole var. ferrotschermakite,
251 magnetite/maghemite and hematite (Table 4). The following phyllosilicates were observed: biotite,

252 muscovite, kaolinite, smectite, illite and chlorite. Mineral quantification showed that minor – but
253 detectable – differences between the different soil horizons and the parent material exist (Table 4).
254 In general, the concentration of clay minerals slightly increased with increasing altitude (fine earth
255 and silt fraction). Phyllosilicate mineralogy also varied as a function of grain size; illites and
256 smectites are more concentrated in the silt than in the fine earth fraction. Illite and smectite nearly
257 doubled in the A-horizons as a function of decreasing grain size. A screening using SEM-EDX
258 confirmed most of the previously described phases. Additionally, traces of apatite and biotite were
259 confirmed under optical microscopy, cathodoluminescence (Fig. 5) and SEM-EDX (data not
260 shown).
261 The cathodoluminescence results were those expected from such phases of granitoid rocks; K-
262 feldspar showed a blue-violet colour, plagioclase a dark green luminescence. CL colours in
263 feldspar were mostly heterogeneous, however some perthitic structures (dark green glow, possibly
264 Na-rich sectors) were scattered throughout most of the samples. The observed broad CL bands for
265 quartz at ca. 450 nm and 650 nm are typical for intrusive quartz. Two emission bands could be
266 observed in the CL spectra of K-feldspar: Al-O^--Al defects (ca. 460 nm; Marfunin, 1979) and the
267 Fe^{3+} impurities substituting Al lattice positions (ca. 700 nm; Götze et al., 2000). Apatite was also
268 detected by its strong (mostly) yellow luminescence emission (Mn^{2+}) and absence of rim (or
269 growing) structures in the crystal, reflecting a homogeneous composition. The emission spectra of
270 apatite (Fig. 5) evidenced sharp emission lines of Dy^{3+}, Nd^{2+}, Sm^{3+} and Eu^{2+} that is typical for
271 apatite originating from alkaline magmatic complexes, and thus relates to the local Precambrian
272 crystalline core (Kempe and Götze, 2002; Dahms, 2004).
273
274 *Dissolution experiments*
275 The majority of dissolved base cations is represented by Ca, Mg and K (about 80-90% of the
276 equivalent concentration); therefore, we focus on these 3 elements. Although the experiment was
277 carried out over 1800 h, constant molar proportions of Ca, Mg and K were established within a
278 relatively short time (Fig. 6). Sodium usually increased within the first hours of the dissolution
279 experiment and then strongly varied around an average, apparent steady state value (data not

280 shown). White and Brantley (2003) reported rather high Na fluctuations due to the presence of
281 fresh and weathered plagioclase dissolution. The results indicate that the weathered plagioclase
282 reached steady-state conditions relative quickly while the reaction rate of fresh plagioclase
283 continued to decrease (White and Brantley, 2003).
284 The total dissolved concentrations in the A-horizon (topsoil) extracts only slightly increased over
285 time, and a steady state was established relatively quickly, when compared to the other
286 experiments (data not shown). Interestingly, the molar ratio of K decreased with increasing altitude
287 (we assume as a function of vegetation type; Fig. 7). Potassium showed highest solute
288 concentrations in A-horizons of soils dominated by sagebrush, followed by forest and tundra. The
289 relative proportion of Ca increased with increasing altitude (Figs. 6 and 7). At the tundra site, Ca
290 concentrations were equal to K (and its equivalent consequently double of that of K). The relative
291 proportion of Mg only slightly increased with altitude. A similar pattern was observed when the A-
292 horizon extracts were added to B-horizon (subsoil) samples from the same ecotone; the molar
293 proportion of K was lower and decreased even more distinctly with increased altitude while the
294 concentration of Ca increased at higher altitude. In general, the molar proportions of Ca measured
295 in the solutions of A- and B-horizons showed distinct increases with altitude and corresponding
296 decreases in K. Mg increased only slightly with altitude. A higher molar proportion of K was
297 measured in A-horizons (and a subsequent lower proportion for Ca) when compared to the B-
298 horizons (Figs. 6, 7 and 8).
299 When the topsoil extract from sagebrush was applied to the forest and tundra sites, again a similar
300 pattern appeared: the concentrations of K decrease with increasing altitude while the molar
301 proportion of Ca increases (Fig. 8). The application of the forest topsoil extract to the tundra soils
302 appears to have caused a further decrease of the molar proportion of K (and a subsequent
303 increase in Ca).
304 Compared to the application of the extract from the forest topsoils on their subsoils, the molar
305 proportion of K increased and those of Ca and Mg decreased when the sagebrush topsoil extract
306 was used on the forest subsoil (Fig. 8). However, the average concentrations of dissolved cations
307 did not change greatly. If we assume a future change to a more forested vegetation distribution in

the tundra ecotone, then a relative increase in K and a corresponding decrease in Ca might be expected (Fig. 8). In the unlikely event of even more drastic warming (e.g. change of the vegetation from tundra to sagebrush), the modelled decrease in the molar proportion of Ca and the corresponding increase in K is even more pronounced; but the equivalent sum of dissolved cations would appear not to change greatly.

Discussion

Soil minerals and chemical properties

Soil pH was lowest at the forest sites, followed by the tundra sites, and then the soils under sagebrush. Even at the sagebrush sites, no carbonates were originally present in the parent material. Thus, along the investigated toposequence, soil pH appears to be distinctly influenced by vegetation as coniferous forest cover often enhances acidification (e.g. Seeber and Seeber, 2005). However, these soils are almost certainly also responding to natural changes in soil moisture content. Since our deepest samples were taken from ~40 cm, the natural increase in MAP and percolation of soil water would steadily remove base cations to lower depths with increased altitude. This process would also help to dissolve/leach extra base cations supplied to the higher-altitude soils via eolian influx, while allowing preferential accumulation at the drier sites under sagebrush (Dahms, 1993; Dahms and Rawlins, 1996).

Although not always statistically different from each other, the organic matter content of the topsoil in the forest and tundra soils were statistically greater than the soils under sagebrush. This seems to agree with trends observed also by other others (e.g., Sadaka and Ponge, 2003): As altitude increases more fresh litter or organic matter is accumulated. Lower temperatures are a main cause of decreased soil microbial activity (Sadaka and Ponge, 2003). The organic matter content in the subsoil significantly increased with increasing altitude, i.e., from sagebrush to forest to tundra (Fig. 4). This trend can be due to two processes: i) increasing podsolization with increasing altitude and subsequent translocation of organic carbon into the subsoil and ii) an increase in root biomass with increasing altitude. It even may be that both processes occur simultaneously. The investigated

336 soils do not a have an extremely low pH. Therefore, they still contain some nutrients. According to
337 Buurman and Jongmans (2005), small accumulation of organic matter in the B horizon occurs in
338 relatively nutrient-rich soils. In Podzols, the subsoil accumulation of organic C is then
339 predominantly due to root input. Loess admixture (that adds nutrients to the soils) may furthermore
340 hinder the podzolization process (Waroszewski et al., 2013). A climate warming (with a
341 subsequent shift in vegetation) consequently could lead to a quite distinct change in soil organic
342 matter storage, as reported also from other alpine environments (Egli et al., 2010). Furthermore,
343 with changing vegetation, also changes in nutrient uptake and cycling (e.g. selective uptake of
344 certain cations) by plants must be assumed (Ponge and Delhaye, 1995).
345 The decomposition of organic matter depends on vegetation and soil type, as well as on faunal
346 and microbial activity (Schinner et al., 1989). Increasing acidification also limits faunal activity,
347 further slowing decomposition, since the soil fauna strongly influences the humification process by
348 creating microhabitats for microorganisms (Brussard and Juma, 1996; Seeber and Seeber, 2005).
349 All these processes lead to the accumulation of organic matter. Leifeld et al. (2013) provided
350 evidence for a strongly differential regulatory role of pH on the turnover of soil organic matter.
351 Mean residence times of soil organic matter fractions significantly increased with declining pH.
352 In general, a trend exists towards higher content of phyllosilicates with altitude (in the fine earth
353 and silt fraction, Table 4). Although these soils may receive a certain aeolian input, the change in
354 mineralogy cannot be explained by this factor because the silt fraction (and in general grain size
355 distribution) of the soils is similar in all ecotones (silt: 33% for the entire soil profile and 38% in the
356 topsoil). Differences are consequently due to weathering processes. The higher phyllosilicate
357 content with increasing altitude is not surprising since the cooler and moister climate of the higher
358 elevation intensifies leaching and weathering. Chemical weathering and mineral transformations
359 are not predominantly limited by low temperatures but are rather controlled by soil moisture (Egli et
360 al., 2014) that is higher at the cooler sites (at higher altitudes where the annual precipitation is also
361 increased). As a consequence of alteration, two important weathering mechanisms can be
362 described (Fig. 9): i) transformation of plagioclase into kaolinite (Fig. 9) and ii) transformation of
363 biotite (significant negative correlation, $p < 0.05$, between the smectite and biotite concentration),

364 and probably also plagioclase into smectite (Fig. 9). Typical for alpine environments, smectite often
365 derives from biotite and/or chlorite as smectite often represents an end-product of mica and/or
366 chlorite weathering (Egli et al., 2003, 2008; Mavris et al., 2011). A part of the newly formed
367 smectite could also to derive from plagioclase (Aoudjit et al., 1995; Bétard et al., 2009). According
368 to Bétard et al. (2009), weathering of plagioclase directly produces illite (Fig. 9) and high-charge
369 smectite ('plagioclase-derived smectite'). Also, at least part of the origin of kaolinite in our soils can
370 be attributed to plagioclase weathering (Fig. 9; Egli et al., 2008).
371 Portions of the mineral content of these soils may have an aeolian origin (Dahms, 1993; Dahms
372 and Rawlins, 1996). The influence of loess deposits can be partially inferred by the quantity of silt
373 and clay in A horizons and the mineralogical composition (Dahms, 1993; Dahms, 2002; Dahms et
374 al., 2010; Dahms et al., 2012). The dominant minerals in loess are usually quartz (Ollier, 1969;
375 Bronger and Heinkele, 1989), mica and kaolinite. The aeolian input is estimated to be in the range
376 of 0.08 to 11.3 g m^{-2} yr^{-1} for parts of the Wind River Range (Dahms and Rawlins, 1996).
377
378 *Weathering and climate change*
379 The solubility of Ca and Mg is kinetically controlled by Ca- and Mg-bearing phases of silicates and
380 phosphates. The dissolution of apatite may represent a source of Ca (Blum et al., 2002). In
381 addition, apatite is the main source of phosphorus. Biotite may contain numerous apatite inclusions
382 (Nezat et al., 2007) which rules the P release to a certain degree. In the presence of biotite, the Fe
383 in biotite may also lock up all of the P immediately. The solubility of P was low and the
384 concentrations remained below the detection limit in our extracted solutions. Thus, we can assume
385 that the solubility of i) Ca is mainly governed by oligoclase, ii) K in part by K-feldspar and in part by
386 biotite and iii) Mg predominantly by mica (i.e., biotite; Table 5). Illite, chlorite and muscovite were
387 also considered as potential sources for soluble Ca, Mg and K. However, when the stoichiometry
388 of all these minerals is used to model the Ca, Mg, K, Na and Al concentrations, then the
389 contribution of illite, chlorite and muscovite to the solubility of Ca, Mg and K seems to be marginal.
390 Amphibole was not taken into consideration because it was barely detectable in the soils.
391 According to Gaillardet et al. (1999), elemental depletion can be better interpreted by considering

both the Ca/Na and the Mg/Na ratios. Many waters draining granitoid bedrock show Ca/Na ratios near 0.9. Gaillardet et al. (1999) while values >> 1 indicate the dissolution of disseminated calcite within granite (Oliva et al., 2004; Mavris et al., 2010).

Tundra topsoils produced Ca/Na ratios of < 1 (Fig. 10). The Ca/Na ratios for solutions of the forest A-horizons were only partially < 1 whereas forested B-horizons were clearly < 1. In the other cases (sagebrush top- and subsoil), the Ca/Na ratios were mostly > 1. Calcium was preferentially mobilised with respect to Na. This leads to higher ratios in the soil water (Ca/Na > 1). When the topsoil solution from forest sites was applied to the subsoil of the tundra sites, the Ca/Na ratio remained close to or below 1. This pattern also held in the cases of the other ecotones when the topsoil solution was applied to another ecotone's subsoil (the Ca/Na was close to or < 1).

As White et al. (2005), Mavris et al. (2010) and others show, decreases in Mg/Na and Ca/Na ratios in soil solutions are related to advanced states of soil weathering. Pore waters from soils of increasing age exhibit decreasing solute concentrations and increasing proportions of Na relative to K, Mg and Ca (White et al., 2005) as well as accelerated Na depletion (Williams et al., 2010). Vegetation change induced by climate warming would be expected to decrease Ca/Na ratios – but not under all conditions. At the tundra sites, a vegetation change to forest cover should tend to lower Ca/Na ratios whereas at the forest sites a change to sagebrush cover should lead to a slight increase in the Ca/Na ratio.

Using our approach, we assume that vegetation exerts a decisive influence on weathering through the interaction of organic ligands with minerals, and that this effect is more important than temperature change. The Arrhenius effect predicts a 1- to 2.3-fold increase in the dissolution rate of plagioclase with a temperature increase from -3.0° to +3.1 °C (using the data and approach of Turner et al., 2010). The assumption that other factors introduced by a change of climate will be decisive for mineral weathering is supported by Lybrand and Rasmussen (2014) across a semiarid environmental gradient in southern Arizona. Their study showed that Na depletion and microscale plagioclase weathering and subsequently-related Si and Na leaching patterns lead to increased silicate weathering in the cooler, wetter, and more biologically productive systems compared to the hot, dry desert scrub system.

Our results show that the relative proportion and, consequently, the importance of K decrease with increasing altitude (Fig. 7). The molar proportion of Ca increases (and the one of Mg remained almost invariable) with altitude and, thus, with a cooler and moister climate. This increase is detected in both the A- and B-horizons (top- and subsoils).

Consequently, the contribution of oligoclase is possibly the most important factor to the overall low- to-high altitude weathering continuum. Because oligoclase also releases Na, the role of both Ca and Na, also will expand. These trends are not limited to climate because of the concurrent and related vegetation changes. Vegetation has a major impact on the biogeochemical cycles of many elements through uptake, re-cycling and the acceleration of weathering rates (e.g. Drever, 1994; Bormann et al., 1998; Hindshaw, 2011). We find that the molar proportion of K decreased with increasing altitude compared to the sum of K, Mg and Ca. We consequently hypothesise that climate warming and vegetation change will lead to an increased molar proportion of K when compared to the other dissolved compounds (Fig. 7). This hypothesis is supported by the experiments where the A-horizon solutions from the sagebrush and forest sites were applied to the sites in the higher altitude ecotones (Fig. 8). Thus, climate warming and a corresponding vegetation change should potentially lead to an increased molar proportion of K (and also Si; Fig. 11) in soils of higher altitudes. The relative importance of K-feldspar weathering should also increase. It is likely that weathering becomes more incongruent under such circumstances, i.e. cations such as K in the interlayer sites of biotite will be preferentially released (Anderson et al., 1997; Blum and Erel, 1997; Hindshaw, 2011). However, since Si is dissolved together with K (Fig. 11), such an incongruent dissolution from biotite interlayers might, in the end, be less important.

A field empirical approach was used in combination with extensive laboratory weathering experiments to simulate several scenarios of climate change. The effects of climate and vegetation changes in a natural environment are known to be complex and any laboratory attempt to reproduce natural conditions is an oversimplification. Nonetheless, the observed trends give at least indications and allow for related hypotheses.

Conclusions

We gained the following insights from our empirical-experimental approach to investigate the potential effects of expected climate and vegetation changes on soils in the Wind River Range:

- The behaviour of the main dissolved cations can be explained by the dissolution of biotite, K-feldspar and oligoclase. With increasing altitude, we found an increase in the relative contribution of oligoclase – and therefore of Ca and Na – to the suite of total dissolved cations in the soil solution.
- We hypothesise that a climate change and a subsequent shift in vegetation - with sagebrush vegetation moving into the present-day forest area and forest or even sagebrush vegetation (unlikely, but …) moving to the present-day tundra zone - will increase the relative contribution of K-feldspar and/or biotite to the suite of dissolved cations. The molar proportion of K would, consequently, also increase.
- Compared to the sagebrush ecotone, the forest and tundra zones exhibit higher soil acidity and slightly higher soil organic matter concentrations. Weathering intensity seems also to increase with higher altitudes. Although a certain part of the soil minerals have an aeolian origin, weathering mechanisms are also reflected by the progressively changing type of phyllosilicates in the soils: biotite is partially transformed to smectite, a portion of the plagioclase is transformed via illite to smectite and some plagioclase also weathers to kaolinite.

A climate and subsequent vegetation change in the dry-alpine region of the Wind River Range seems to exert several modifications in the biogeochemistry of the soils. This regards the dissolution behaviour of the main primary minerals and the subsequent solubility and leaching of associated elements and suggests that potassium will play a major role in future element cycles of such environments.

Acknowledgments

475 This project was granted by the Swiss National Foundation for Science (SNF project n.
476 PBZHP2_141452) and supported by the Department of Geography (University of Northern Iowa).
477 The authors wish to thank to Dr. John DeGroote for the support with the GIS datasets and maps,
478 Prof. Diane McKnight for providing the environmental chamber, Fabian Züst for the help during
479 field work and everybody who helped with fruitful discussions during the analytical and drafting
480 process of this work.
481
482
483 **References**
484 Adams, H.D., Guardiola-Claramonte, M., Barron-Gafford, G.A., Villegas, J.C., Breshears, D.D.,
485 Zou, C.B., Troch, P.A., Huxman, T.E., 2009. Temperature sensitivity of drought-induced tree
486 mortality portends increased regional die-off under global-change type drought. Proceedings of
487 the National Academy of Sciences USA 10, 7063-7066.
488 Aoudjit, H., Robert, M., Elsass, F., Curmi, P., 1995. Detailed study of smectite genesis in granite
489 saprolites by analytical electron microscopy. Clay Minerals 30, 135-148.
490 Amundson, R., Richter, R.R., Humphreys, G.S., Jabbagy, E., Gaillardet, J., 2007. The coupling
491 between biota and earth materials in the critical zone. Elements 3, 327-332.
492 Anderson, S. P., Drever, J. I., Humphrey, N. F. 1997. Chemical weathering in glacial environments.
493 Geology 25, 399-402.
494 Arn, K., 2002. Geochemical weathering in the sub- and proglacial zone of two glaciated crystalline
495 catchments in the Swiss Alps (Oberaar- and Rhoneglacier). Ph.D. Thesis, University of
496 Neuchâtel, Neuchâtel, Switzerland.
497 Berthel, N., Schörer, C., Tinner, W., 2012. Impact of Holocene climate changes on alpine and
498 treeline vegetation at Sanetsch Pass, Bernese Alps, Switzerland. Review of Palaeobotany and
499 Palynology 174, 91-100.
500 Bétard, F., Caner, L., Gunnell, Y., Bourgeon, G., 2009. Illite neoformation in plagioclase during
501 weathering: evidence from semi-arid Northeast Brazil. Geoderma 152, 53-62.
502 Blum, D., Erel, Y., 1997. Rb-Sr isotope systematics of a granitic soil chronosequence: The

503 importance of biotite weathering. Geochimica et Cosmochimica Acta 61, 3193–3204.
504 Blum, J.D., Klaue, A., Nezat, C.A., Driscoll, C.T., Johnson, C.E., Siccama, T.G., Eagar, C., Fahey,
505 T.J., Likens, G.E., 2002. Mycorrhizal weathering of apatite as an important calcium source in
506 base-poor forest ecosystems. Nature 417, 729-731.
507 Bormann, B. T., Wang, D., Bormann, F. H., Benoit, G., April, R., Snyder, M. C., 1998. Rapid, plant
508 induced weathering in an aggrading experimental ecosystem. Biogeochemistry 43, 129–155.
509 Bradford, J.B., Schlaepfer, D.R., Lauenroth, W.K., 2014. Ecohydrology of Adjacent Sagebrush and
510 Lodgepole Pine Ecosystems: The Consequences of Climate Change and Disturbance.
511 Ecosystems 17, 590-605.
512 Brantley, S.L., Megonigal, J.P., Scatena, F.N., Balogh-Brunstad, Z., Barnes, R.T., Bruns, M.A.,
513 Van Cappellen, P., Dontsova, K., Hartnett, H.E., Hartshorn, A.S., Heimsath, A., Herndon, E.,
514 Jin, L., Keller, C.K., Leake, J.R., McDowell, W.H., Meinzer, F.C., Mozdzer, T.J., Petsch, S.,
515 Pett-Ridge, J., Pregitzer, K.S., Raymond, P.A., Riebe, C.S., Shumaker, K., Sutton-Grier, A.,
516 Walter, R., Yoo, K., 2011. Twelve testable hypotheses on the geobiology of weathering.
517 Geobiology 9, 140-165.
518 Bronger, A., Heinkele, T., 1989. Paleosol sequences as witnesses of Pleistocene climatic history.
519 In: Bronger, A., Catt, J.A. (Eds.), Paleopedology – Nature and Applications of Paleosols. Catena
520 Supplement 16, pp. 163-186.
521 Brussard, L., Juma, N.G., 1996. Organisms and humus in soils. In: Piccolo, A. (Ed.), Humic
522 Substances in Terrestrial Ecosystems. Elsevier, Amsterdam, pp. 329– 356.
523 Buurman, P., Jongmans, A.G., 2005. Podzolisation and soil organic matter dynamics. Geoderma
524 125, 71-83.
525 Christidis, G.E., Blum, A.E., Eberl, D.D., 2006. Influence of layer charge and charge distribution of
526 smectites on the flow behavior and swelling of bentonites. Applied Clay Science 34, 125-138.
527 Dahms, D.E., 1993. Mineralogical evidence for eolian sediments in soils on Late Quaternary
528 moraines, Wind River Mountains, Wyoming. Geoderma 59,175-196.
529 Dahms, D.E., 2002. Glacial stratigraphy of Stough Creek basin, Wind River Range, Wyoming.
530 Geomorphology 42, 59-83.

531 Dahms, D.E., 2004. Relative and Numeric Age Data for Pleistocene Glacial Deposits and
532 Diamictons in and near Sinks Canyon, Wind River Range, Wyoming, U.S.A. Arctic, Antarctic,
533 and Alpine Research 36, 59-77.
534 Dahms, D.E., Rawlins, C.L., 1996. A two-year record of eolian sedimentation in the Wind River
535 Range, Wyoming, U.A.A. Arctic and Alpine Research 28, 210-216.
536 Dahms, D.E., Birkeland, P.W., Shroba, R.R., Miller, C. Dan, Kihl, R., 2010. Latest Quaternary
537 Glacial and Periglacial Stratigraphy, Wind River Range, Wyoming. Geological Society of
538 America, Digital Maps and Charts Series #7, 46 p., doi: 10.1130/2010.DMCH007.
539 Dahms, D., Favilli, F., Krebs, R., Egli, M., 2012. Soil weathering and accumulation rates of oxalate-
540 extractable phases derived from alpine chronosequences up to 1 Ma in age. Geomorphology
541 151-152, 99-113.
542 Dean, W.E., 1974. Determination of carbonate and organic matter in calcareous sediments and
543 sedimentary rocks by loss on ignition: comparison with other methods. Journal of Sedimentary
544 Petrology 44, 242-248.
545 Di Pasquale, G., Marziano, M., Impagliazzo, S., Lubritto, C., De Natale, A., Bader, M.Y., 2008. The
546 Holocene treeline in the northern Andes (Ecuador): First evidence from soil charcoal.
547 Palaeogeography, Palaeoclimatology, Palaeoecology 259, 17-34.
548 Dixon, J.L., Heimsath, A.M., Anmundson, R., 2009. The critical role of climate and saprolite
549 weathering in landscape evolution. Earth Surface Processes and Landforms 34, 1507-1521.
550 Drever, J. I., 1994. The effect of land plants on weathering rates of silicate minerals. Geochimica
551 Cosmochimica Acta 58, 2325–2332.
552 Eberl, D.D., 2004. Quantitative mineralogy of the Yukon River system: Changes with reach and
553 season, and determining sediment provenance. American Mineralogist 89, 11-12, 1784-1794.
554 Egli, M., Mirabella, A., Fitze, P., 2003. Formation rates of smectites derived from two Holocene
555 chronosequences in the Swiss Alps. Geoderma 117, 81-98.
556 Egli, M. Mirabella, A., Sartori, G., Fitze, P. 2003. Weathering rates as a function of climate: results
557 from a climosequence of the Val Genova (Trentino, Italian Alps). Geoderma 111, 99-121.

558 Egli, M., Mirabella, A., Sartori, G. 2008. The role of climate and vegetation in weathering and clay
559 mineral formation in late Quaternary soils of the Swiss and Italian Alps. Geomorphology 102,
560 307-324.
561 Egli, M., Sartori, G., Mirabella, A., 2010. The effects of exposure and climate on the weathering of
562 late Pleistocene and Holocene Alpine soils. Geomorphology 114, 466-482.
563 Egli, M., Lessovaia, S., Chistyakov, K., Inozemzev, S., Polekhovsky, Y., Ganyushkin, D., 2014.
564 Microclimate affects soil chemical and mineralogical properties of cold-alpine soils of the Altai
565 mountains (Russia). Journal of Soils and Sediments, DOI 10.1007/s11368-013-0838-4.
566 Erslev, E.A., 1986. Basement balancing of Rocky Mountain foreland uplifts. Geology 14, 259-262.
567 Fabel, D., Harbor, J., Dahms, D., James, A., Elmore, D., Horn, L., Daley, K., Steele, C., 2004.
568 Spacial patterns of glacial erosion at a valley scale derived from terrestrial cosmogenic ^{10}Be and
569 ^{26}Al concentrations in Rocks. Annals of the Association of American Geographers 94, 2, 241-
570 255.
571 Frost, B.R., Frost, C.D., Hulsebosch, T.P., Swapp, S.M., 2000. Origin of the chamockites of the
572 Louis Lake batholith, Wind River Range, Wyoming. Journal of Petrology 41, 1759-1776.
573 Furrer, G., Sollins, P., Westall, P., 1990. The study of soil chemistry through quasi-steady-state
574 models. II. Acidity of soil solution. Geochimica et Cosmochimica Acta 54, 2363-2374.
575 Gaillardet, J., Dupré, B., Louvat, P., Allègre, C.J., 1999. Global silicate weathering and CO_2
576 consumption rates deduced from the chemistry of large rivers. Chemical Geology 159, 3-30.
577 Götze, J., Krbetschek, M.R., Habermann, D., Wolf, D., 2000. High-resolution cathodoluminescence
578 of feldspar minerals. In: Pagel, M., Barbin, V., Blanc, Ph., Ohnenstetter, D. (eds.),
579 Cathodoluminescence in geosciences. Springer Verlag, Berlin Heidelberg New York Tokyo, pp.
580 245-270.
581 Heimsath, A.M., DiBiase, R.A., Whipple, K.X., 2012. Soil production limits and the transition to
582 bedrock-dominated landscapes. Nature Geoscience 5, 210–214.
583 Heimsath, A.M., 2014. Limits of soil production? Science 343, 617-618.
584 Heiri, O., Lotter, A.F., Lemcke, G., 2001. Loss on ignition as a method for estimating organic and
585 carbonate content in sediments: reproducibility and comparability of results. Journal of

586 Paleolimnology 25, 101-110.
587 Hindshaw, R.S., 2011. Chemical weathering and calcium isotope fractionation in a glaciated
588 catchment. PhD tesis, Diss. ETH No. 19778, Zurich.
589 Hosein, R., Arn, K., Steinmann, P., Adatte, T., Föllmi, K.B., 2004. Carbonate and silicate
590 weathering in two presently glaciated, crystalline catchments in the Swiss Alps. Geochimica et
591 Cosmochimica Acta 68, 1021–1033.
592 Jacobson, A.D., Blum, J.D., 2003. Relationship between mechanical erosion and CO2
593 consumption in the New Zealand Southern Alps. Geology 31, 865–868.
594 Jann, B., 2005. Einführung in die Statistik. 2., bearbeitete Auflage. München: Oldenburg
595 Wissenschaftsverlag.
596 Kempe, U., Götze, J., 2002. Cathodoluminescence (CL) behaviour and crystal chemistry of apatite
597 from rare-metal deposits. Mineralogical Magazine 66, 151-172.
598 Larsen, J.L., Almond, P.C., Eger, A., Stone, J.O., Montgomery, D.R., Malcolm, B., 2014. Rapid soil
599 production and weathering in the Southern Alps, New Zealand. Science 343, 637-640.
600 Leifeld, J., Bassin, S., Conen, F., Hajdas, I., Egli, M., Fuhrer, J., 2013. Control of soil pH on
601 turnover of belowground organic matter fractions in subalpine grasslands. Biogeochemistry 112,
602 59-69.
603 Love, J.D., Christiansen, A.C., Ver Ploeg, A.J., 1992. Stratigraphic nomenclature chart for
604 Wyoming. Geological Survey of Wyoming Open-File Report 92-2, 1 sheet.
605 Love, J.D., Christiansen, A.C., 1985. Geologic map of Wyoming, Map scale 1:500,000. U.S.
606 Geological Survey.
607 Lybrand, R.A., Rasmussen, C., 2014. Linking soil element-mass-transfer to microscale mineral
608 weathering across a semiarid environmental gradient. Chemical Geology 381, 26–39.
609 Marfunin, A.S., 1979. Spectroscopy, Luminescence and Radiation Centers in Minerals. Springer-
610 Verlag, Berlin.
611 Massatti, R.T., 2007. A floristic inventory of the east slope of the Wind River Mountain Range and
612 vicinity, Wyoming. PhD Thesis, University of Wyoming, ProQuest, UMI Dissertations Publishing.
613 Mavris, C., Egli, M., Plötze, M., Blum, J.D., Mirabella, A., Giaccai, D., Haeberli, W., 2010. Initial

614 stages of weathering and soil formation in the Morteratsch proglacial area (Upper Engadine,
615 Switzerland). Geoderma 155, 359-371.
616 Mavris, C. Plötze, M., Mirabella, A., Giaccai, D., Valboa, G., Egli, M., 2011. Clay mineral evolution
617 along a soil chronosequence in an Alpine proglacial area. Geoderma, 165, 106-117.
618 Muhs, D.R., Bettis, E.A., Been, J., McGeehin, J.P., 2001. Impact of climate and parent material on
619 chemical weathering in loess-derived soils of the Mississippi river valley. Soil Science Society of
620 America Journal 65, 1761-1777.
621 Neuser, R.D., Bruhn, F., Götze, J., Habermann, D., Richter, D.K., 1995. Kathodolumineszenz:
622 Methodik und Anwendung. Zentralblatt für Geologie und Paläontologie Teil I, H. 1/2, 287-306.
623 Nezat, C.A., Blum, J.D., Yanai, R.D., Hamburg, S.P., 2007. A sequential extraction to determine
624 the distribution of apatite in granitoid soil mineral pools with application to weathering at
625 Hubbard Brook Experimental Forest, NH, USA. Applied Geochemistry 22, 2406-2421.
626 Oliva, P., Dupré, B., Martin, F., Viers, J., 2004. The role of trace minerals in chemical weathering in
627 a high-elevation granitic watershed (Estibère, France): Chemical and mineralogical evidence.
628 Geochimica et Cosmochimica Acta 68, 2223-2244.
629 Ollier, C.D., 1969. Weathering. Oliver & Boyd, Edinburgh, Scotland.
630 Óskarsson, B.V., Riishuus, M.S., Arnalds, O., 2012. Climate-dependent chemical weathering of
631 volcanic soils in Iceland. Geoderma 189-190, 635-651.
632 Ponge, J.F., Delhaye, L., 1995. The heterogeneity of humus profiles and earthworm communities
633 in a virgin beech forest. Biology and Fertility of Soils 20, 24-32.
634 PRISM Climate Group, 2014. Annual average precipitation (1981-2010). Oregon State University.
635 Rasmussen, C., Brantley, S.L., Richter, D., Blum, A., Dixon, J., White, A., 2011. Strong climate
636 control on plagioclase weathering in granitic terrain. Earth and Planetary Science Letters 301,
637 521-530.
638 Riebe, C.S., Kirchner, J.W., Finkel, R.C., 2004. Erosional and climatic effects on long-term
639 chemical weathering rates in granitic landscapes spanning diverse climate regimes. Earth and
640 Planetary Science Letters 224, 547–562.
641 Sadaka, N., Ponge, J.F., 2003. Climatic effects on oil trophic networks and the resulting hums

642 profiles in holm oak (Quercus rotundifolia) forests in the High Atlas of Morocco as revealed by
643 correspondence analysis. European Journal of Soil Science 54, 767-777.
644 Schinner, F., Hofmann, J., Niederbacher, R., 1989. Mikrobielle Aktivitäten des
645 Kohlenstoffmetabolismus im Boden der alpinen, subalpinen und montanen Stufe des
646 Grogglocknergebietes (Hohe Tauern). In: Cernusca, A. (Ed.), Veröffentlichungen des
647 Österreichischen MaB-HochgebirgsprogrammsHohe Tauern, Band 13. Universitätsverlag
648 Wagner, Innsbruck, pp. 257–262.
649 Schoeneberger, P.J., D.A. Wysocki, E.C. Benham, and Soil Survey Staff. 2012. Field book for
650 describing and sampling soils, Version 3.0. Natural Resources Conservation Service, National
651 Soil Survey Center, Lincoln, NE.
652 Seastedt, T.R., Bowman, W.D., Caine, T.N., McKnight, D., Townsend, A., Williams, M.W., 2004.
653 The landscape continuum: A model for high-elevation ecosystems. BioScience 54, 111-121.
654 Seeber, J., Seeber, G.U.H., 2005. Effects of land-use changes on humus forms on alpine
655 pastureland (Central Alps, Tyrol). Geoderma 124, 21-–222.
656 Singer, M.J., Janitzky, P., 1986. Field and Laboratory Procedures used in a Soil Chronosequence
657 Study. U.S. Geological Survey Bulletin 1648. U.S. Govt Print. Off., Washington.
658 Soil Survey Staff. 2014. Keys to Soil Taxonomy, 12th ed. USDA-Natural Resources Conservation
659 Service, Washington, DC.
660 Solàr, J., 2013. Effect of climate change on mountain pine distribution in western Tatra Mountains.
661 In: Singh, B.R. (ed.), Climate Change – Realities, Impacts Over Ice Cap, Sea Level and Risks.
662 InTech, pp. 437-458.
663 Stumm, W., Morgan, J.J., 1996. Aquatic chemistry. Third edition. John Wiley and Sons, Inc., New
664 York.
665 Sverdrup, H., Warfvinge, P., 1993. Calculating field weathering rates using a mechanistic
666 geochemical model PROFILE. Journal of Applied Geochemistry 8, 273 - 283.
667 Theurillat, J.P., Felber, F., Geissler, P., Gobat, J.M., Fierz, M., Fischlin, A., Küpfer, P., Schlüssel,
668 A., Velluti, C., Zhao, G.-F., Williams, J., 1998. Sensitivity of plant and soil ecosystems of the
669 Alps to climate change. In: Cebon, P., Dahinden, U., Davies, H.C., Imboden, D., Jaeger, C.C.

(Eds.), Views from the Alps. MIT Press, Massachusetts, pp. 225–308.

Turner, B.F., White, A.F., Brantley, S.L., 2010. Effects of temperature on silicate weathering: Solute fluxes and chemical weathering in a temperate rain forest watershed, Jamieson Creek, British Columbia. Chemical Geology 269, 62-78.

Waroszewski, J., Kalinski, K., Malkiewicz, M., Mazurek, R., Kozlowski, G., Kabala, C., 2013. Pleistocene–Holocene cover-beds on granite regolith as parent material for Podzols — An example from the Sudeten Mountains. Catena 104, 161-173.

Wehrli, B., Wieland, E., Furrer, G., 1990. Chemical mechanisms in the dissolution kinetics of minerals; the aspect of active sites. Aquatic Sciences 52, 3-31.

Wells, A.F., Boettinger, J.L., Houston, K.E., Roberts, D.W., in press. Ecological Types of the Eastern Slope of the Wind River Range, Shoshone National Forest, Wyoming. General Technological Report RMRS-GTR-XXX- Fort Collins, Colorado. U.S. Department of Agriculture, Forest Service, Rocky Mountain Research Station.

White, A.F., Blum, A.E., 1995. Effects of climate on chemical weathering in watersheds. Geochimica et Cosmochimica Acta 59, 1729-1747.

White, A.F.. Brantley, S.L., 2003. The effect of time on the weathering of silicate minerals: why do weathering rates differ in the laboratory and field? Chemical Geology 202, 479 – 506.

White, A.F., Blum, A.E., Bullen, T.D., Vivit, D.V., Schulz, M., Fitzpatrick, J., 1999. The effect of temperature on experimental and natural chemical weathering rates of granitoid rocks. Geochimica et Cosmochimica Acta 63, 3277–3291.

White, A.F., Schulz, M.S., Vivit, D.V., Blum, A.E., Stonestrom, D.A., Harden, J.W., 2005. Chemical weathering rates of a soil chronosequence on granitic alluvium: III. Hydrochemical evolution and contemporary solute fluxes and rates. Geochimica et Cosmochimica Acta 69, No. 8, pp. 1975–1996.

Williams, J.Z., Bandstra, J.Z., Pollard, D., Brantley, S.L., 2010. The temperature dependence of feldspar dissolution determined using a coupled weathering–climate model for Holocene-aged loess soils. Geoderma 156, 11–19.

Wise, D.U., 1963. Keystone faulting and gravity sliding driven by basement uplift of Owl Creek

698 Mountains, Wyoming. American Association of Petroleum Geologists Bulletin 47, 586-598.
699 Zanelli, R., Egli, M., Fitze, P., Giaccai, D., Mirabella, A. 2006. Influence of laurophyllous species,
700 chestnut and native vegetation on organic matter in soils in Southern Switzerland and Northern
701 Italy. Geoderma, 136, 723-737.
702 Zanelli, R., Egli, M., Mirabella, A., Giaccai, A., Abdelmoula, M. 2007. Vegetation effects on
703 pedogenetic forms of Fe, Al and Si and on clay minerals in soils in southern Switzerland and
704 northern Italy. Geoderma 141, 119-129.
705 Züst, F., Dahms, D. Purves, R., Egli, M., 2014. Surface reconstruction and derivation of erosion
706 rates over several glaciations (1 Ma) in an alpine setting. Geomorphology, 219, 232-247.

Table 1
Click here to download Table: Table1.doc

Table 1. Characteristics of the field sites.

Ecotone	Vegetation	Elevation	MAT[1)]	MAP[1)]	Soils (Soil Taxonomy; Soil Survey Staff, 2014)	Parent material
		m asl	°C	mm/yr		
Sagebrush	Mountain big sagebrush/bluebunch wheatgrass; with *Artemisia tridentata* var. *vaseyana*/, *Elymus spicatus, Elymus spicatus-Poa secunda*	2400	+2.7	400	Ustic Argicryoll	Granitic till
Forest	Douglas-fir with Rocky Mountain maple whitebark pine/grouse whortleberry; *Pinus albicaulis*/*Vaccinium scoparium* h.t. as dominant species	3200	-2.1	700 - 800	Ustic Haplocryoll	Granitic till
Tundra	Blackroot sedge, Alpine Turf; with *Geum rossii* var. *turbinatum* as the dominant species	3350	-3.0	800 - 900	Typic Haplocryoll	Granitic till

[1)] Data source: Massatti (2007), Dahms et al. (2012), PRISM Climate Group (2014)

Table 2

Click here to download Table: Table2.doc

Table 2. Characteristics of the soils of the sagebrush (S) ecological type zone.

Site	horizon	depth (cm)	sampled[1]	skeleton (wt %)	grain size (wt %)			LOI[2] (wt %)	pH ($CaCl_2$)
					sand	silt	clay		
S1	(O)A	0 - 4	A	15.7	56.1	35.4	8.5	2.0	4.4
	B	4 - 34+	B	15.3	59.0	35.5	5.5	1.4	4.7
S2	O	0 - 2	A[3]	9.9	45.3	54.7	0.0	2.6	5.0
	A	2 – 5							
	B	5 - 40+	B	32.0	66.8	26.2	6.9	0.8	4.9
S3	O	0 – 2	A	11.7	56.8	30.1	13.1	3.0	5.2
	A	2 - 6							
	B	6 - 40+	B	20.8	68.3	25.4	6.3	1.1	5.4
S4	(O)A	0 - 6	A	15.5	51.8	39.4	8.9	4.2	4.9
	B	6 - 38+	B	18.7	67.4	27.4	5.3	1.2	5.2
S5	(O)A	0 - 6	A	15.4	60.4	32.9	6.7	2.8	5.3
	B	6 - 40+	B	28.4	69.0	23.0	7.9	1.1	5.4
S6	O	0 - 3	A	15.6	59.0	31.4	9.6	2.8	5.1
	A	3 - 7							
	B	7 - 40+	B	26.4	63.5	28.8	7.7	1.1	5.3
S7	O	0 - 1	A	18.2	62.1	30.1	7.9	3.2	5.0
	A	1 - 3							
	B	3 - 40+	B	29.0	72.2	24.0	3.8	0.9	5.2
S8	O	0 - 2	A	11.5	54.9	34.4	10.7	2.6	5.1
	A	2 - 5							
	B	5 - 30+	B	32.7	63.0	28.9	8.1	1.4	5.4
S9	O	0 - 2	A	10.7	66.7	33.2	0.0	3.8	5.2
	A	2 - 6							
	B	6 - 30+	B	26.4	65.6	27.8	6.5	1.1	5.3
S10	O	0 - 1	A	12.3	54.1	35.0	10.9	2.6	5.2
	A	1 - 4							
	B	4 - 38+	B	14.9	40.4	43.0	16.5	2.3	5.3
S11	OA	0 - 4	A	19.1	60.6	32.0	7.4	4.1	5.1
	B	4 - 40+	B	31.0	72.4	21.9	5.7	0.5	5.1
S12	OA	0 - 6	A	17.8	69.5	30.5	0.0	3.3	5.1
	B	6 - 35	B	26.3	68.8	29.1	2.1	0.7	4.5
	C	35+	C	37.9	72.3	27.7	0.0	0.4	4.5
S13	O	0 - 2	A	9.6	53.7	33.8	12.4	2.9	5.7
	A	2 - 15							
	B	15 - 35	B	57.3	63.9	31.3	4.7	1.5	5.6
	C	35 - 40+	C	60.9	76.1	19.3	4.6	0.7	5.4
S14	O	0 - 2	A	23.0	47.6	44.2	8.2	2.2	4.8
	A	2 - 8							
	B	8 - 25	B	16.8	54.5	37.0	8.5	1.4	4.6
	C	25+	C	20.2	59.2	40.3	0.5	1.1	5.0
S15	O	0 - 1	A	17.5	61.0	29.9	9.2	2.2	5.0
	A	1 - 8							
	Bw	8 - 30	Bw[4]	61.7	67.7	28.7	3.7	1.0	4.9
	BC	30 - 40	BC	49.9	75.2	16.0	8.9	0.8	5.0
	C?	40+	C?	n.s./n.m.[5]	n.s./n.m.	n.s./n.m.	n.s./n.m.	n.s./n.m.	n.s./n.m.
S16	OA	0 - 15	A	25.8	51.1	37.7	11.2	3.2	n.a.
	Bw1	15 - 30	Bw1	16.3	61.7	27.0	11.3	1.1	5.3
	Bw2	30 - 40+	Bw2	18.9	63.8	33.7	2.4	1.1	5.5
S17	O	0 - 6	A	17.0	55.4	36.2	8.4	4.6	5.4
	A	6 - 15							
	Bw1	15 - 30	Bw1	18.1	67.7	32.3	0.0	0.6	5.1
	Bw2	30+	Bw2	41.1	72.6	27.4	0.0	0.5	5.1
S18	O	0 - 2	A	18.9	57.2	34.8	8.0	3.5	5.3
	A	2 - 10							
	B	10 - 35	B	22.2	63.0	33.2	3.7	1.1	5.5
	BC/Cox	35+	BC/Cox	n.s./n.m.	n.s./n.m.	n.s./n.m.	n.s./n.m.	n.s./n.m.	n.s./n.m.
S19	O1	0 - 3	A	25.0	61.0	36.9	2.1	3.9	4.3

	O2								
	A	3 - 8							
	B	8 - 16	B	21.8	62.2	37.8	0.0	1.1	4.8
	BC	16 - 38	BC	n.s./n.m.	n.s./n.m.	n.s./n.m.	n.s./n.m.	n.s./n.m.	n.s./n.m.
	C	38+	C	28.4	84.8	14.3	1.0	0.6	4.9
S20	O	0 - 5	A	3.4	46.2	47.0	6.8	2.9	5.4
	A	5 - 10							
	Bt	10 - 35+	B	1.8	32.8	55.1	12.1	1.8	5.1

[1] final sampling according to the aim of the mineral weathering study;
[2] loss on ignition, calculated by weight loss after calcination at 550 °C (organic matter, OM) and 950 °C (carbonates); the difference between the two steps is zero, thus the resulting values are related to volatilization of OM;
[3] values for A horizons include bulk sampling of O, A, and E horizons
[4] when more than one B horizons were detected, the upper one was considered
[5] not sampled/not measured

Table 3

Click here to download Table: Table3.doc

Table 3. Characteristics of the soils of the forest- (F) and tundra- (T) dominated ecological type zone.

Site	horizon	depth (cm)	sampled[1]	skeleton (wt %)	grain size (wt %)			LOI[2] (wt %)	pH ($CaCl_2$)
					sand	silt	clay		
F1	O	0 – 2	A[3]	18.9	50.6	41.7	7.7	4.7	3.6
	A	2 – 9							
	E	9 – 15							
	Bhs	15 – 22	B[4]	40.2	58.1	32.0	9.9	2.0	4.1
	Bs	22 – 40							
	BC	40+	BC	n.s./n.m.[5]	n.s./n.m.	n.s./n.m.	n.s./n.m.	n.s./n.m.	n.s./n.m.
F2	O	0 – 2	A	11.2	52.9	47.1	0.0	5.5	4.2
	A	2 – 9							
	E	9 – 12							
	Bs	12 – 30	B	29.0	69.8	20.8	9.4	1.5	4.0
	BC	30 – 40	C	n.s./n.m.	n.s./n.m.	n.s./n.m.	n.s./n.m.	n.s./n.m.	n.s./n.m.
	C	40+		n.s./n.m.	n.s./n.m.	n.s./n.m.	n.s./n.m.	n.s./n.m.	n.s./n.m.
F3	O	0 – 1	A	28.4	51.4	45.4	3.2	3.1	3.5
	A	1 – 4							
	E	4 – 6							
	Bs	6 – 28	B	39.0	65.7	29.7	4.6	1.4	4.1
	BC	28+	C	n.s./n.m.	n.s./n.m.	n.s./n.m.	n.s./n.m.	n.s./n.m.	n.s./n.m.
F4	O	0 – 3	A	16.2	58.7	30.8	10.4	2.2	3.5
	A	3 – 9							
	E	9 – 18							
	Bs	18 - 30+	B	43.8	73.4	22.3	4.3	2.1	4.0
F5	O	0 – 4	A	7.6	71.7	20.9	7.4	1.7	4.2
	A	4 – 9							
	E	9 – 14							
	Bws	14 – 25	B	5.9	61.2	21.4	17.4	1.6	4.0
	Bs	25 - 40+	BS	n.s./n.m.	n.s./n.m.	n.s./n.m.	n.s./n.m.	n.s./n.m.	n.s./n.m.
F6	O	0 – 5	A	4.9	44.6	49.8	5.6	3.9	4.0
	AE	5 – 15							
	Bs1	15 – 32	Bs1	36.1	69	25.9	5.1	1.7	4.2
	Bs2	32+	Bs2	n.s./n.m.	n.s./n.m.	n.s./n.m.	n.s./n.m.	n.s./n.m.	n.s./n.m.
F7	OA	0 – 10	A	27.3	64.5	35.5	0.0	2.1	4.2
	E	10 – 18							
	Bs	18 - 40+	B	15.9	71.1	23.5	5.3	0.9	4.3
F8	O	0 – 2	A	9.7	57.4	37.0	5.5	5.8	4.2
	OA	2 – 6							
	AE	6 – 10							
	Bs	10 - 30+	B	n.s./n.m.	50.4	44.1	5.5	2.4	3.9
F9	O	0 – 5	A	5.4	68.1	26.2	5.6	5.4	3.8
	OA	5 – 9							
	E	9 – 12							
	Bw	12 – 16	Bw	15.1	74.3	25.0	0.8	1.1	3.8
	2Bs	16 - 30+	2Bs	n.s./n.m.	n.s./n.m.	n.s./n.m.	n.s./n.m.	n.s./n.m.	n.s./n.m.
F10	O	0 – 2	A	8.6	39.1	48.4	12.5	4.6	3.8
	OA	2 – 7							
	E	7 – 10							
	Bw	10 - 30+	B	5.8	46.5	43.2	10.3	1.5	3.8
T1	OA	0 – 12	A	6.0	55.6	30.6	13.9	3.4	5.0
	Bw	12 – 25	B	55.7	67.0	33.0	0.0	1.9	4.4
	BC	25+	BC	50.9	84.6	15.4	0.0	0.9	4.2
T2	OA	0 – 8	A	9.1	59.4	31.2	9.3	4.0	4.9

	(A)B	8 – 10							
	Bw	10 - 35+	B	9.5	59.9	27.8	12.2	1.5	4.8
T3	O	0 – 2	A	8.0	63.6	26.1	10.3	2.0	4.5
	A	2 – 10							
	E	10 – 18							
	Bws	18 – 40	B	9.7	65.1	24.8	10.2	1.6	4.0
T4	O	0 – 1	A	5.0	47.8	37.4	14.8	3.8	4.0
	A	1 - 8							
	B	8 - 35+	B	6.9	50.0	42.1	7.9	1.7	4.5
T5	O	0 – 2	A	4.2	42.3	57.4	0.3	4.8	4.9
	A	2 – 7							
	B	7 - 40+	B	7.6	54.4	29.3	16.4	2.1	4.6
T6	A	0 – 8	A	12.3	55.6	39.6	4.9	5.0	4.9
	Bw	8 – 20	B	18.2	66.3	29.8	7.0	2.6	4.5
	BC	20+	BC	n.s./n.m.	n.s./n.m.	n.s./n.m.	n.s./n.m.	n.s./n.m.	n.s./n.m.
T7	A	0 – 8	A	5.7	46.0	48.6	1.8	4.9	4.8
	Bw	8 – 20	B	44.5	63.2	29.8	7.0	2.2	4.5
	BC	20+	BC	n.s./n.m.	n.s./n.m.	n.s./n.m.	n.s./n.m.	n.s./n.m.	n.s./n.m.
T8	A	0 – 10	A	2.5	46.0	41.9	12.1	4.0	5.2
	AB	10 - 15							
	Bw	15 – 35	B	18.0	61.6	26.9	11.6	2.9	5.0
	BC	35+	BC	n.s./n.m.	n.s./n.m.	n.s./n.m.	n.s./n.m.	n.s./n.m.	n.s./n.m.
T9	A	0 – 4	A	19.0	44.1	47.0	9.0	8.5	4.8
	AB	4 – 10	B	18.4	74.0	22.3	3.7	1.2	3.8
	Bw/Bs	10 - 35+	Bw/Bs	43.8	58.0	34.5	7.5	2.2	4.4
T10	A	0 – 12	A	10.3	49.2	50.8	0.0	2.8	5.3
	Bw	12 - 28	B	31.6	73.9	20.0	6.1	2.2	5.0
	BC (Cox)	28+	BC	n.s./n.m.	n.s./n.m.	n.s./n.m.	n.s./n.m.	n.s./n.m.	n.s./n.m.

[1] final sampling according to the aim of the mineral weathering study;
[2] loss on ignition, calculated by weight loss after calcination at 550 °C (organic matter, OM) and 950 °C (carbonates); the difference between the two steps is zero, thus the resulting values are related to volatilization of OM;
[3] values for A horizons include bulk sampling of O, A, and E horizons
[4] when more than one B horizons were detected, the upper one was considered
[5] not sampled/not measured

Table 4

Click here to download Table: Table4.doc

Table 4. Mineralogical composition (composite samples from all soil pits) of the fine earth and silt fractions in horizons of each ecotone.

	Fine earth fraction (< 2mm)							Silt fraction (2 - 63 µm)					
Site	S		F		T			S		F		T	
Horizon	A	B	A	B	A	B	C	A	B	A	B	A	B
Main minerals													
Quartz	31	32	25	31	26	31	32	33	37	27	29	29	30
K-feldspar	17	15	14	17	13	19	15	13	14	14	13	13	14
Plagioclase	28	33	20	30	26	28	33	17	19	22	17	16	21
Amphibole	< 1	< 1	< 1	< 1	< 1	< 1	< 1	< 1	< 1	< 1	< 1	< 1	< 1
Magnetite/Maghemite	2	2	< 1	< 1	< 1	< 1	2	< 1	< 1	1	1	< 1	1
Hematite	< 1	< 1	< 1	< 1	< 1	< 1	< 1	< 1	< 1	< 1	< 1	< 1	< 1
Amorphous, organic	13	5	25	9	21	11	10	18	10	16	15	20	16
Total main minerals	90	88	85	89	86	90	94	82	83	81	77	79	83
Phyllosilicates													
Kaolinite	< 1	< 1	< 1	< 1	< 1	1	0	< 1	< 1	1	2	1	2
Smectite	3	3	9	3	6	3	< 1	5	3	5	6	8	4
Illite	4	3	3	3	3	2	2	8	7	5	7	5	4
Biotite	1	2	< 1	1	< 1	< 1	2	1	2	2	1	1	1
Chlorite	< 1	< 1	< 1	1	< 1	< 1	< 1	< 1	2	2	4	2	1
Muscovite	2	3	2	3	3	3	2	4	4	4	4	4	4
Total phyllosilicates	10	12	15	11	14	10	6	18	18	19	23	21	17

S = sagebrush, F = forest, T = tundra

Table 5
Click here to download Table: Table5.doc

Table 5. A simplified model of mineral contribution to the dissolved cations assuming congruent dissolution.

Vegetation type	Sagebrush			Forest			Tundra		
	Ca (µmol/L)	Mg (µmol/L)	K (µmol/L)	Ca (µmol/L)	Mg (µmol/L)	K (µmol/L)	Ca (µmol/L)	Mg (µmol/L)	K (µmol/L)
average conc.	107.2	41.9	221.2	91.4	39.8	113.6	57.1	21.7	65.7
Mineral contribution to dissolution									
Biotite		41.9	14.0		39.8	13.3		21.7	7.2
K-Fspar			207.2			100.4			58.4
Oligoclase	107.2			91.4			57.1		

Biotite: $KMg_3AlSi_3O_{10}(OH)_2$
K-Fsp: $KAlSi_3O_8$
Oligoclase: $(Na_{0.8}Ca_{0.2})Al_{1.2}Si_{2.8}O_8$ (according to mindat; http://www.mindat.org/); in a more general form: $(Na_{1-x}Ca_x)Al_{1.2}Si_{2.8}O_8$

Figure captions

Fig. 1. Overview of the WRR sampling areas, located in the U.S. state of Wyoming (inset): (a) Sinks Canyon (20 sagebrush sites), and (b) Stough Creek Basin (10 forest and 10 tundra sites).

Fig. 2. Typical scenes in the three ecotones: (a) tundra, (b) forest, and (c) sagebrush.

Fig. 3. Scheme of the set-up for the batch experiments. Topsoil (A) aqueous extracts of the three ecotones sagebrush (S), forest (F), and tundra (T) were made: S(A), F(A) and T(B). In addition, the topsoil extracts were reacted with the solid fine earth samples from the subsoils of the same ecotones and from the higher altitude ecotones: the topsoil extract S(A) was merged with S(B), F(B) and T(B), the topsoil extract F(A) with F(B) and T(B), and the topsoil extract T(A) with T(B).; for a total of six topsoil extract-subsoil combinations. In addition each topsoil was reacted with deionised water, adding three more combinations to the batch experiments.

Fig. 4. Box plot of soil pH and LOI (loss on ignition) of the fine soil material from topsoil (A) and subsoil (B) for each ecotone, and from parent materials (C) from some random location.

Fig. 5. Thin sections of the bulk parent material (two examples are given). The transmitted light (left) is compared to the hot cathodoluminescence-irradiated sample (right). Mineral phases were found to be quartz (Qtz), plagioclase (Plg), K-feldspar (Kfs), biotite (Bi), and traces of apatite (Apa). Below, cathodoluminescence spectra with the relevant activators of the main minerals and apatite are given.

Fig. 6. Molar ratios of Ca ([Ca]/([Ca]+[Mg]+[K])), Mg ([Mg]/([Ca]+[Mg]+[K])) and K ([K]/([Ca]+[Mg]+[K])) over time and as a function of the experimental set-up: (first row) topsoil extracts of the three ecotones sagebrush (S), forest (F), and tundra (T): S(A), F(A) and T(A), (second row) topsoil extracts merged with the solid subsoil samples (S(B), F(B) and T(B)) from the

same ecotone, (third row) topsoil extracts merged with the solid subsoil samples from the higher altitude ecotones: S(A) with F(B) and T(B), and F(A) with T(B).

Fig. 7. Average molar ratios of Ca, Mg and K in the topsoil extracts as a function of ecotone and consequently altitude.

Fig. 8. Average molar ratios of Ca, Mg and K in the batch experiments for the subsoils receiving the extracts from the corresponding topsoil; S(A) → S(B) for sagebrush, F(A) → F(B) for forest, T(A) → T(B) for tundra and in the subsoils receiving the extracts from the topsoils of the lower altitude ecotones S(A) → F(B), F(A) → T(B), and S(A) → T(B)).

Fig. 9. Relationships between plagioclase and the sheet silicates illite, smectite and kaolinite (fine earth and silt fraction; data in Table 4). Error probability is for all data: $p < 0.05$.

Fig. 10. Ca/Na vs. Mg/Na molar ratios for extracts and as a function of the different experiments: only topsoil extracts of the S, F and T sites (left), topsoil extracts applied on the corresponding subsoils (middle) and (right) transfer of topsoil extracts to the subsoils of the higher elevated sites (right; with S(A) → F(B): sagebrush topsoil extract applied on the subsoil of the forest site; S(A) → T(B): sagebrush topsoil extract applied on the subsoil of the tundra site; F(A) → T(B): forest topsoil extract applied on the subsoil of the tundra site).

Fig. 11. Chemical composition of the extracts represented in ternary plots. Only topsoil extracts of S, F and T (left), topsoil extracts applied on the corresponding subsoils (middle) and transfer of topsoil extracts to the subsoils of the higher elevated sites (right; with S(A) → F(B): sagebrush topsoil extract applied on the subsoil of the forest site; S(A) → T(B): sagebrush topsoil extract applied on the subsoil of the tundra site; F(A) → T(B): forest topsoil extract applied on the subsoil of the tundra site).

Figure 1

Click here to download high resolution image

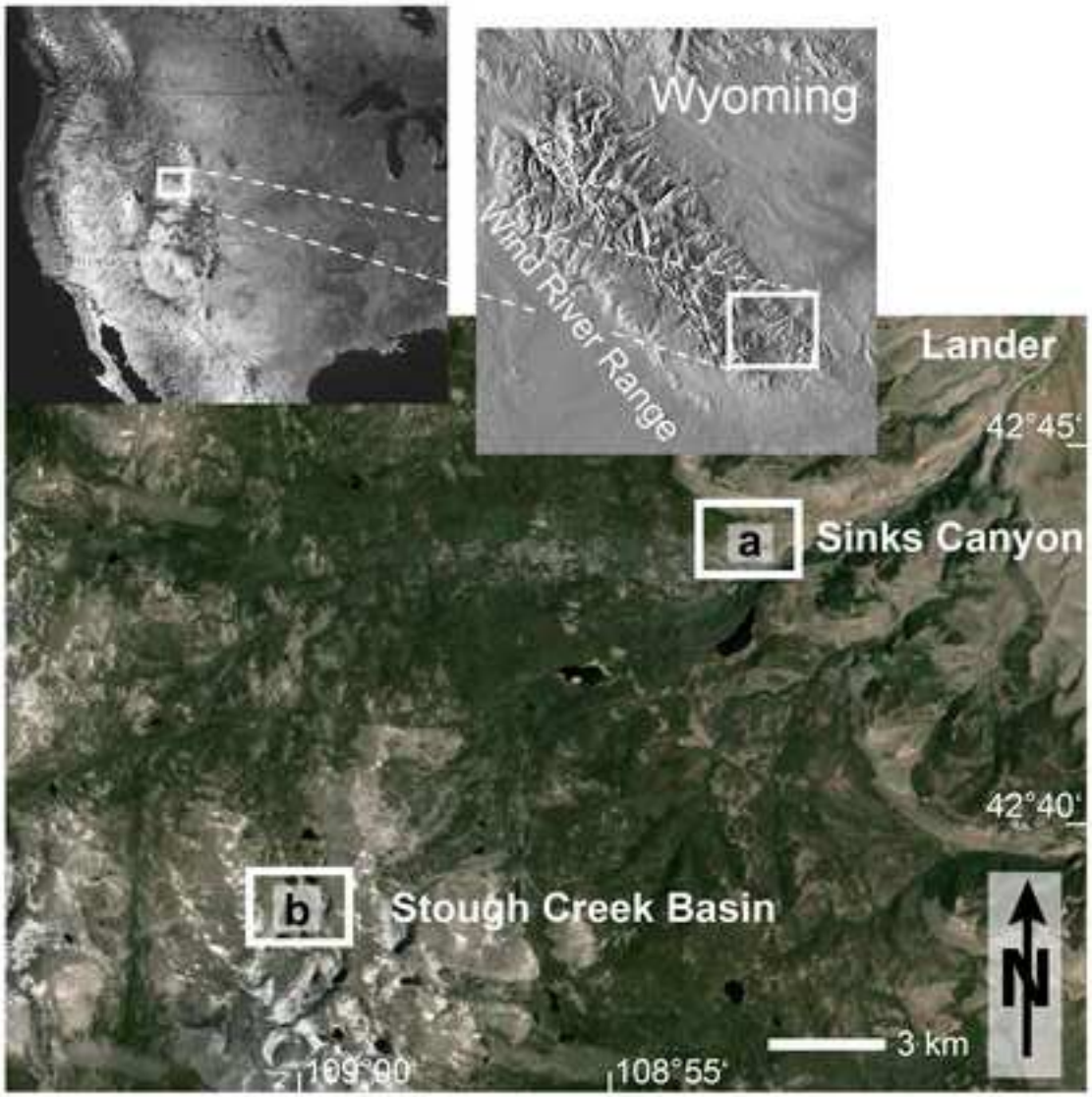

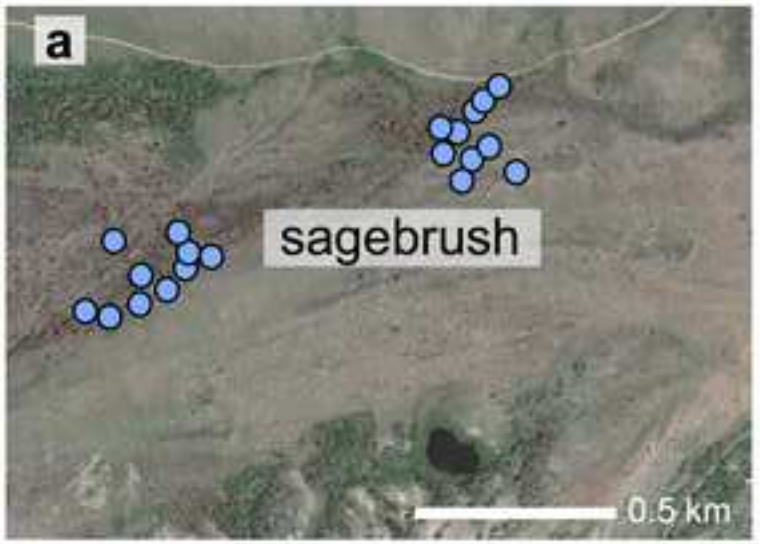

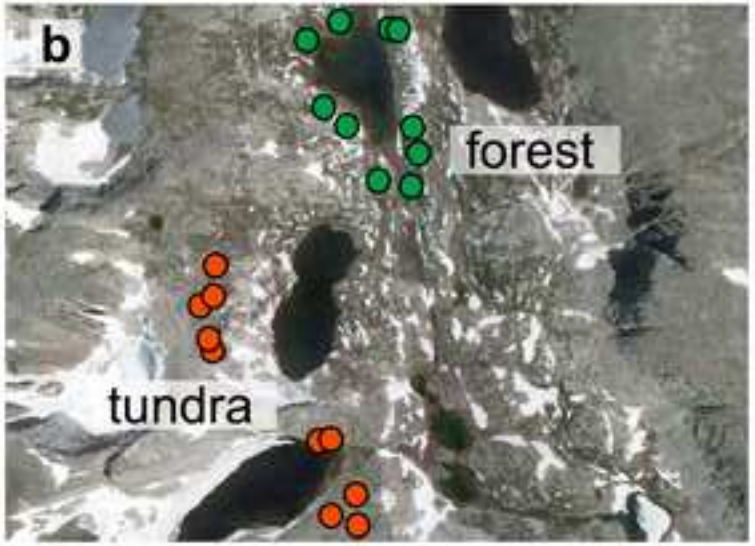

Figure 2

Click here to download high resolution image

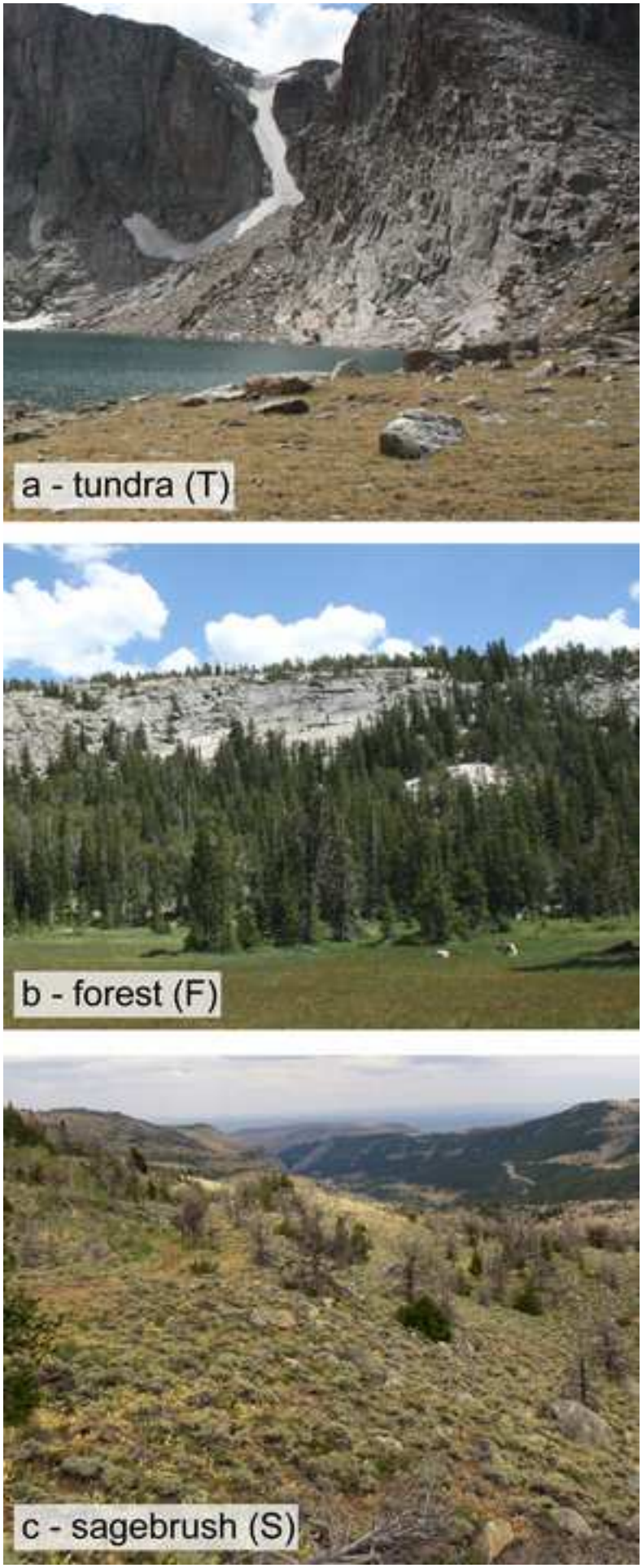

Figure 3

Click here to download high resolution image

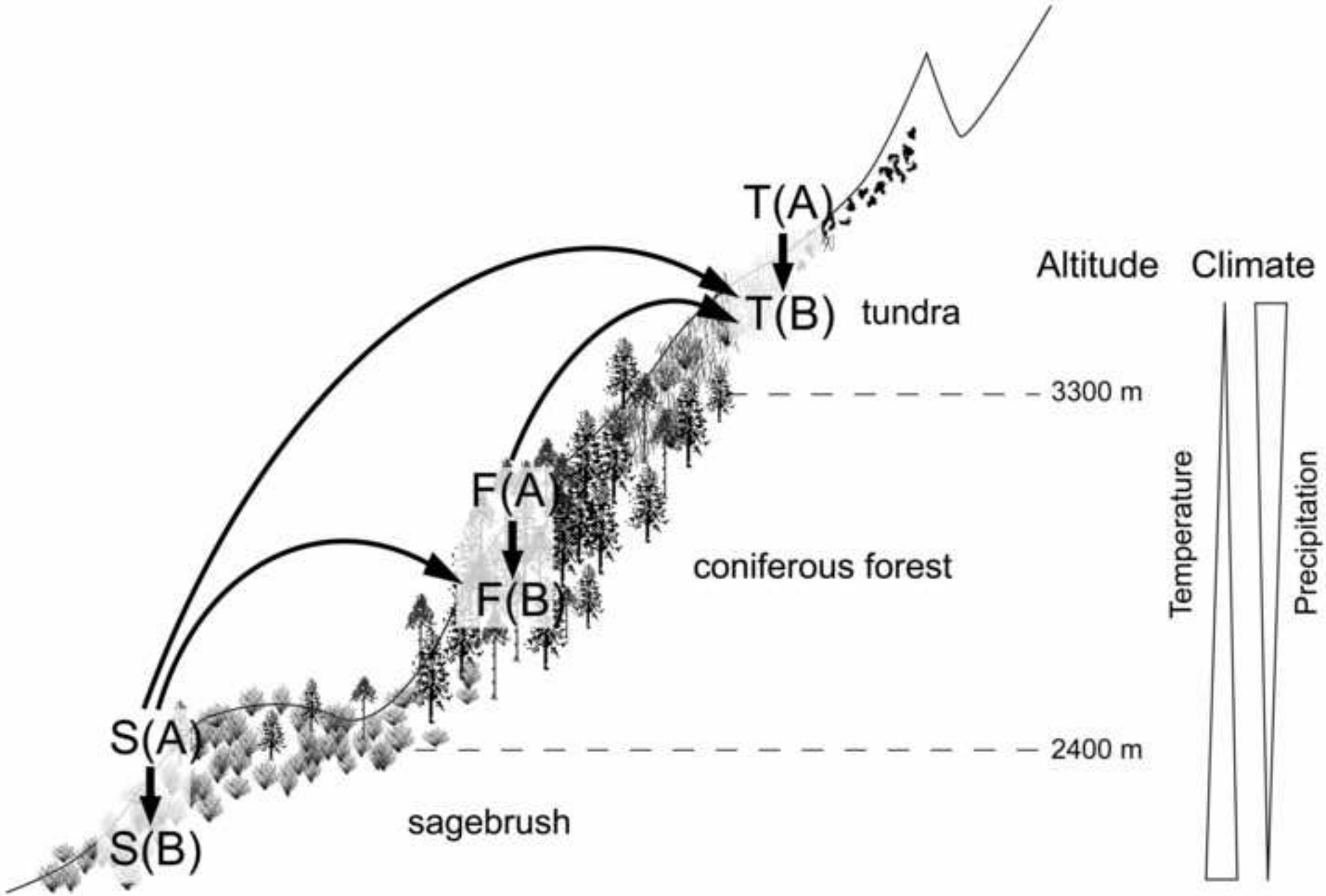

Figure 4

Click here to download high resolution image

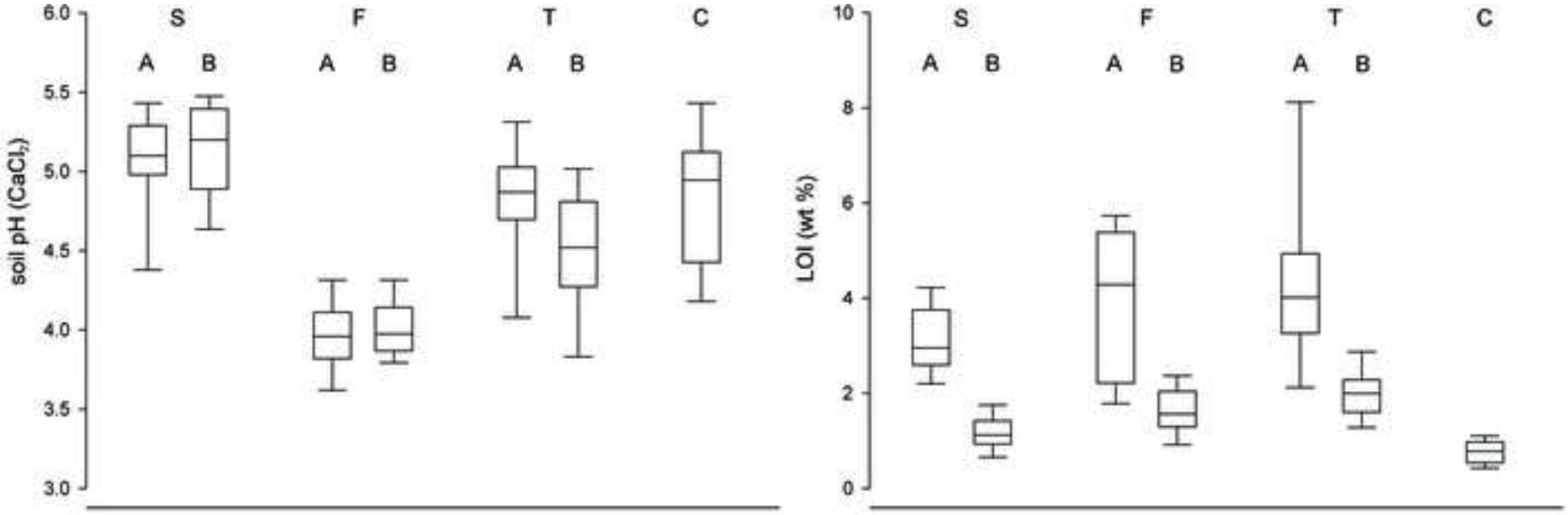

Figure 5

Click here to download high resolution image

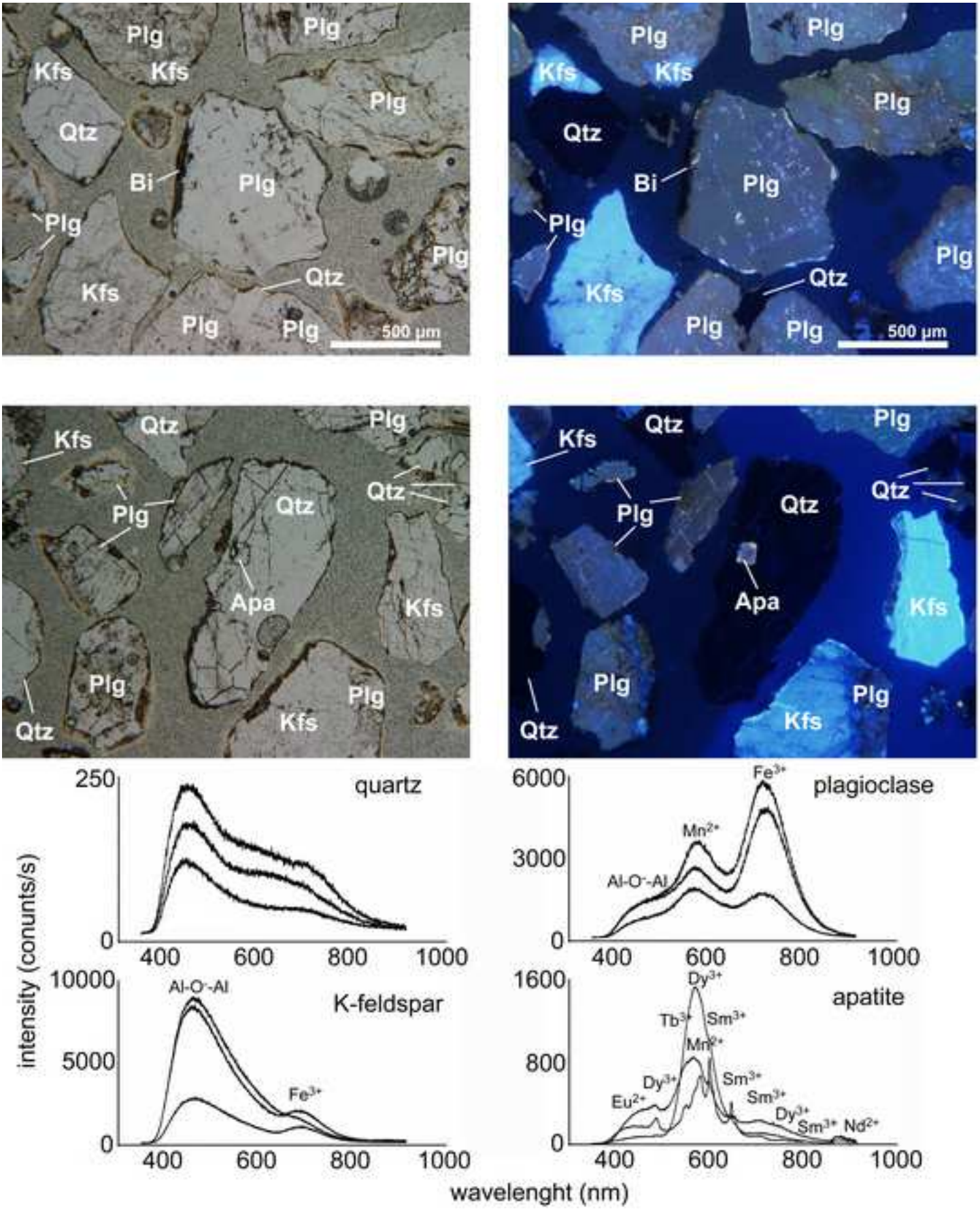

Figure 6

Click here to download high resolution image

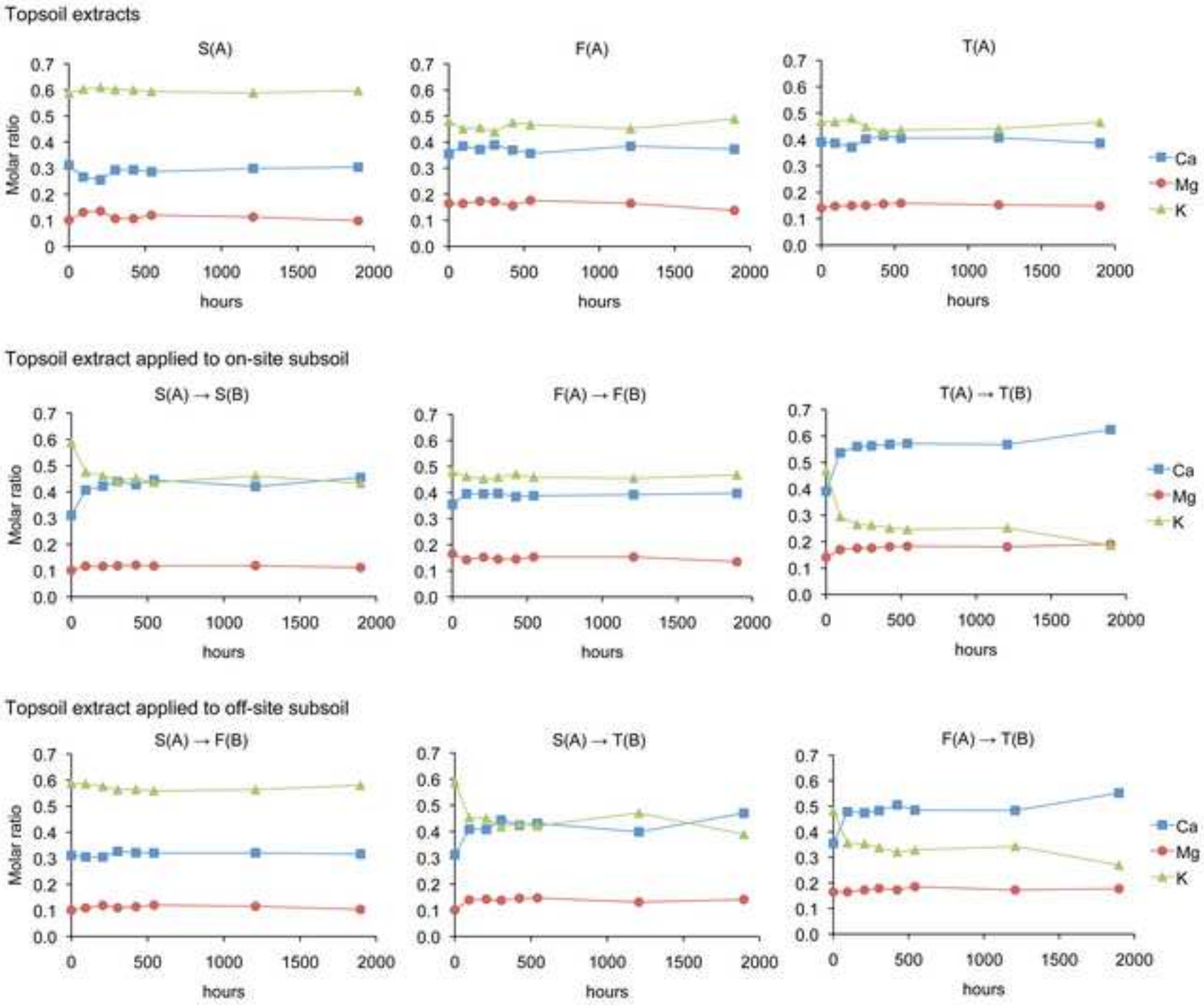

Figure 7

Click here to download high resolution image

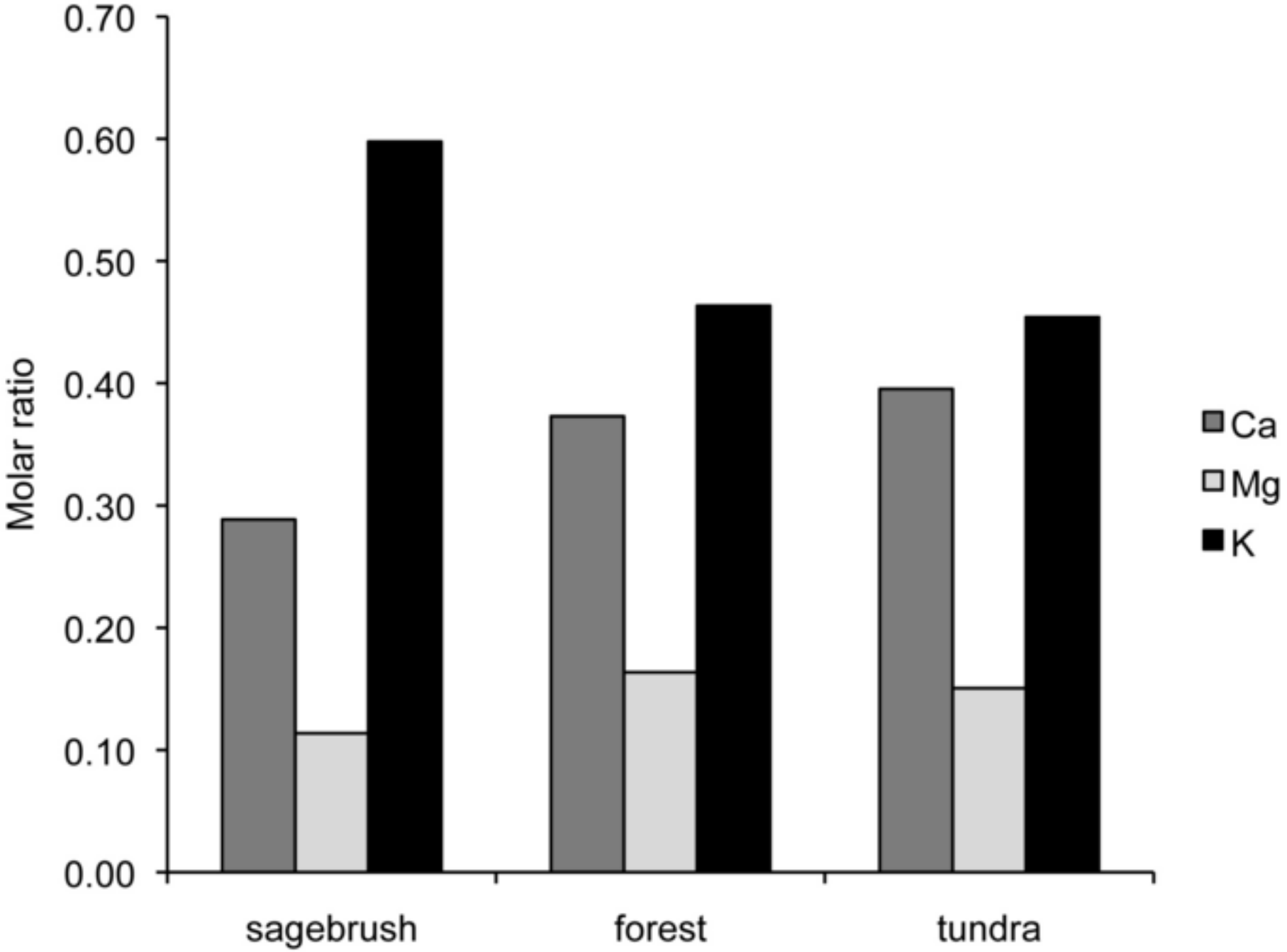

Figure 8

Click here to download high resolution image

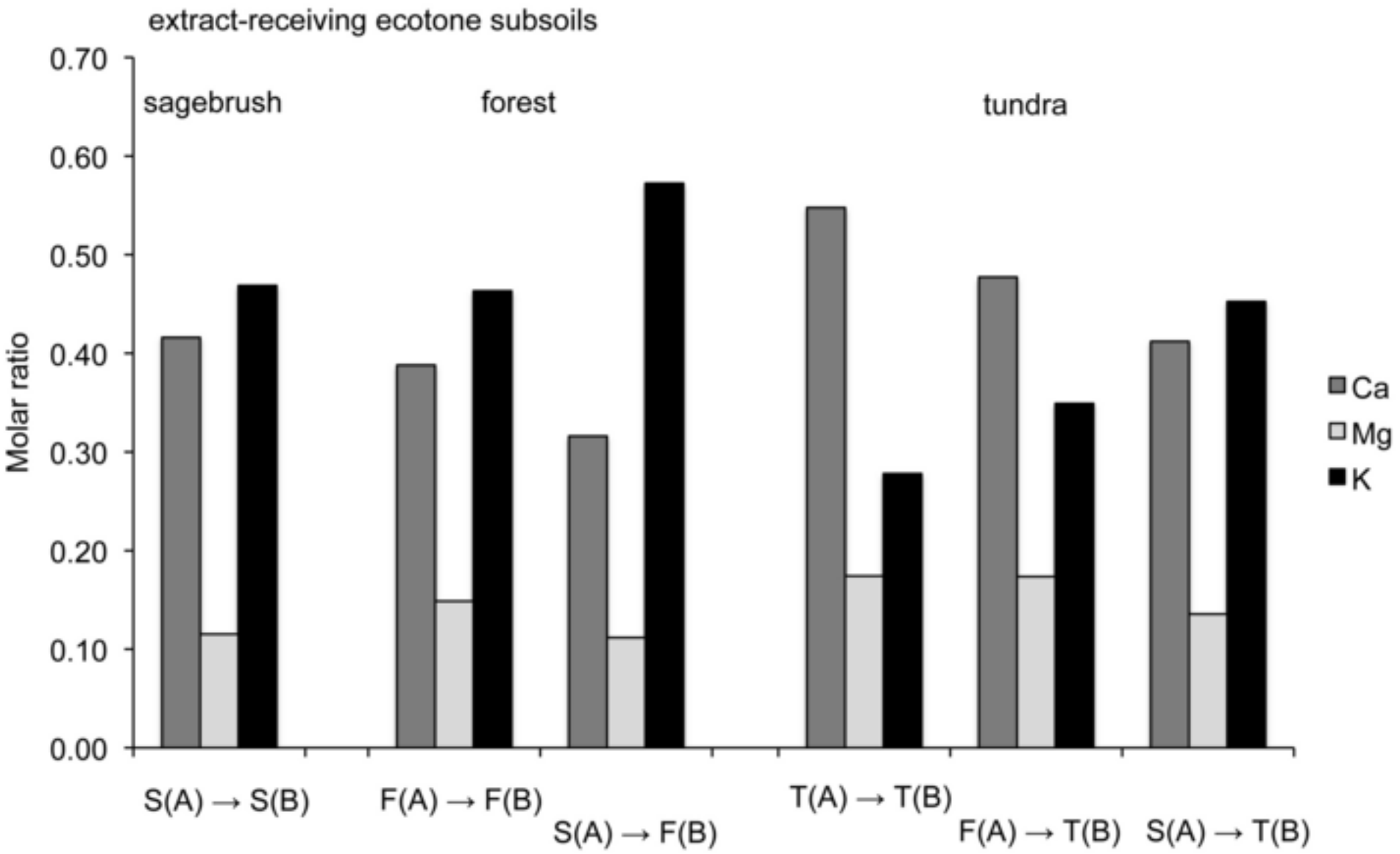

Figure 9

Click here to download high resolution image

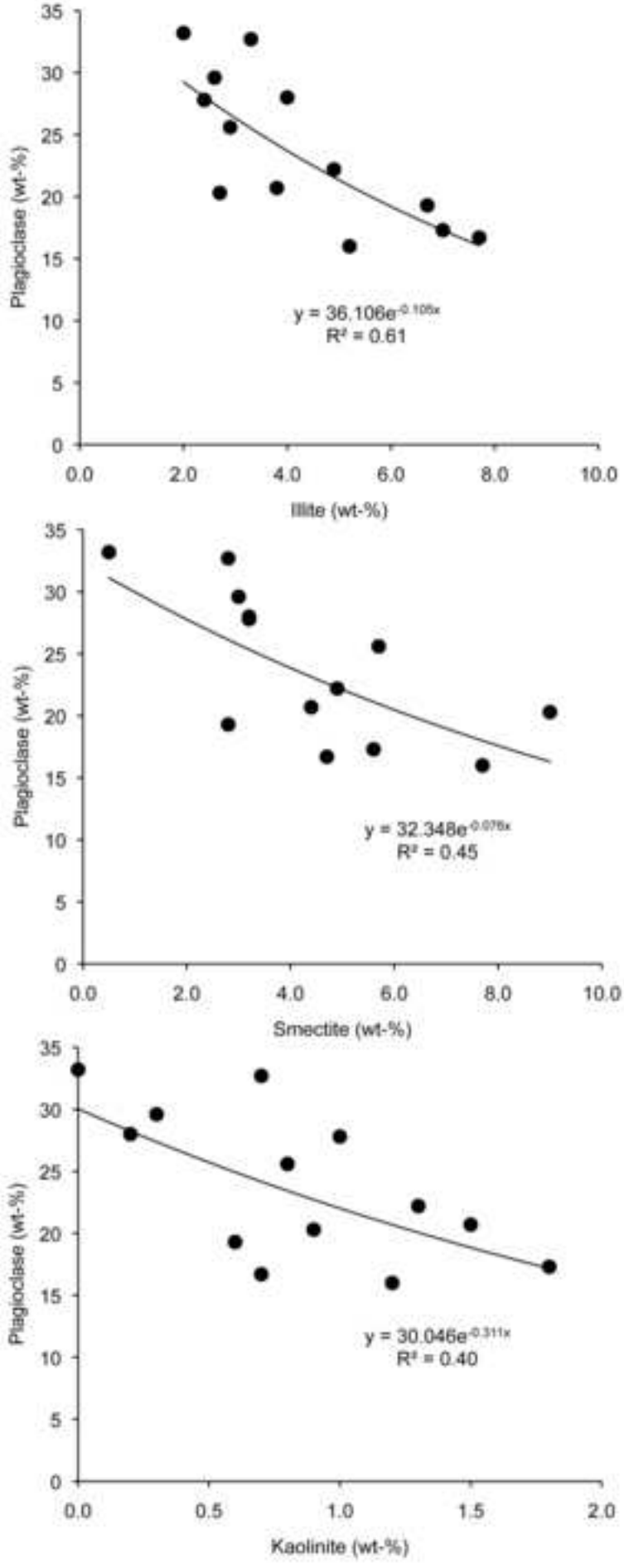

Figure 10

Click here to download high resolution image

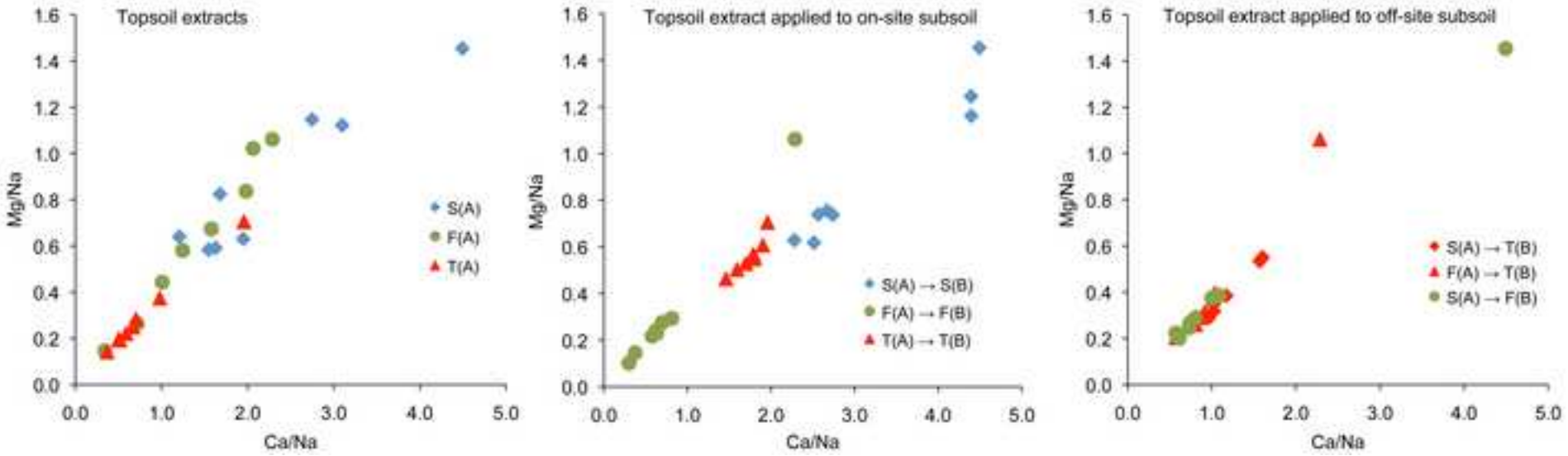

Figure 11

Click here to download high resolution image